Depositional history and pockmarks in Vartdalsfjorden, Sunnmøre

Anna Svendal Aase
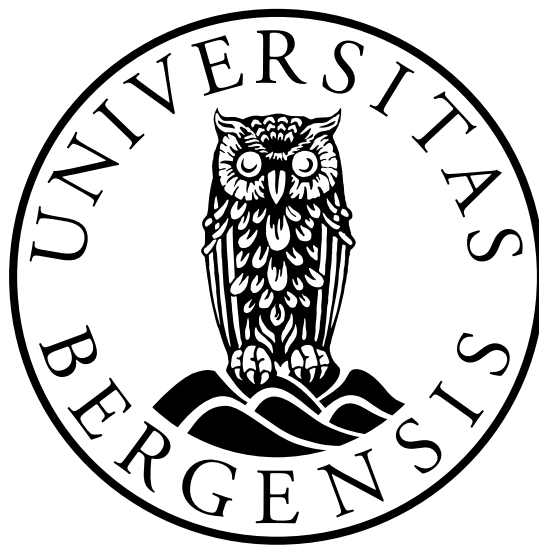
Master thesis in Earth Science

Department of Earth Science

University of Bergen

September, 2022

Abstract

In Vartdalsfjorden, Sunnmøre, 19 pockmarks have been observed in connection with the road authorities ferry free E39 project. Pockmarks are indications of seepage of fluids or gas in the sediment. The pockmarks in Vartdalsfjorden have an average diameter of 45 m, a depth of around 1 m and a relief between 3-7 %. The formation age of the pockmarks is between 3.8-6.6 cal ka BP. Determining the formation mechanisms and whether or not the pockmarks are active or inactive is important in order to assess potential hazards for seabed installations. However, a limited amount of research have been done on pockmarks in Norwegian fjords. Here we show the results from seismiostratigraphy, chronostratigraphy, microbial taxonomy and pore water analysis which indicate that there is some evidence of gas in the sediments. Bright spots on the seismic (line 4) was observed indicating presence of gas. In addition, a bacterial mat was observed, however no evidence of gas or fluids escaping where observed from the microbial taxonomy and pore water analysis. This indicates that the most likely formation mechanisms for the pockmarks in Vartdalsfjorden is release of shallow gas, either periodical or during events.

Acknowledgement

Contents

1. Introduction

In the middle part of Vartdalsfjorden, Sunnmøre, around 20 pockmarks have been identified recently. The pockmarks are located in the middle of the basin and are around 50 m in diameter and around 1 m deep. Some of these pockmarks are located in an area close to where the proposed foundation for a bridge is planned in conjunction with the road authorities project ferry free E39.

Fjord basins are efficient sediment traps during deglaciations, but also during interglacials and interstadial phases. The west Norwegian fjords are a result of glacier erosion along weakness zones in the bedrock and former fluvial valleys (Aarseth, 1997). The fjords are recognised by their steep relief both above and below sea level. A water depth between 500-700 m are common and all fjords have a sill of 200-300 m water depth. Some fjords have several bedrock or moraine sills (Aarseth, 1997). By studying the sediments in the fjord it is possible to get an understanding of the formation mechanisms for the pockmarks.

The occurrence and location of the pockmarks are an indication of fluid flow in the sediments. Whether the pockmarks are active or not is important to determine since active pockmarks can potentially destabilise the sediments around the seafloor installation. Therefore, it is important to study the area and collect data about the geological processes behind the pockmark formation in Vartdalsfjorden.

So far pockmarks have only been observed in fjord sediments as an exception, which makes these structure in Vartdalsfjorden extra interesting for research. Several hypotheses have been presented as possible explanations for pockmarks of this demeanour. One hypothesis is that there is a release of ground water either from a bedrock structure or from bottom sediments. Another is the possibility that they are formed by shallow gas from buried organic rich sediments, which seeps out either during episodic or certain events.

Pockmarks are in need of further research, and a limited number of areas have been explored. Research have been done at Svalbard (Spitsbergen) ((Forwick et al., 2009); (Roy et al., 2015)), the Oslofjorden and Scotland and there are used for the background in this study. Forwick et al. (2009) utilised swath bathymetry and high-resolution seismic data to analyse pockmarks in Spitsbergen fjords. They located pockmarks in Grønfjorden, Ymerbukta, Ad-

ventfjorden, Billefjorden and van Keulenfjorden which had a width up to 250 m and a depth of 13 m. These pockmarks are a result of seepage of thermogenic gas and pore water fluids.

Roy et al. (2015) analysed the pockmark morphology and their spatial distribution in Isfjorden relative to seabed morphology, bedrock geology, fault systems, glacial landforms and processes using multibeam bathymetric data. In the study a total of 1304 pockmarks were detected between a depth of 40 - 320 m, and they varied between circular and elongated in plan-view. The diameter range from 14 to 265 m with depths from 1 to 11 m. In the Isfjordbanken and outer Isfjorden elongated pockmarks dominated and here the seafloor was influenced by a current (West Spitsbergen Current) (Roy et al., 2015).

In Lochs of western Scotland 1019 structures were interpreted both as circular and elongated pockmarks. The majority of the circular pockmarks are located within the approach of the fjord or the glaciated bays. These pockmarks have been interpreted based on three factors. First they only occur in the seabed sediment, second their morphology is similar to pockmarks that have been mapped elsewhere on the European shelf sea, and last the pockmarks are associated with regions of acoustic or gas blanking in the seismic records (Audsley et al., 2019).

1.1 Objectives of the study

One of the objectives for this thesis is to create a depositional history for Vartdalsfjorden by studying the seismostratigraphy, core stratigraphy and dating to create a basis for the chronostratigraphy.

The main objectives of this study are to unveil the formation mechanisms of the pockmarks in Vartdalsfjorden, and whether they are active or inactive today. This is done by combining stratigraphic, sedimentological, seismic data, geochemical and microbial community analyses of two sediment cores, one collected within and one outside one of the pockmarks. The sub objective for this study is:

- Determine the formation age for the pockmarks

- Research whether there is seepage of gas or fresh water

2. Background

2.1 Study site

Vartdalsfjorden is a narrow fjord located in Hareid, Ulstein and Ørsta municipality in Møre and Romsdal county (Fig.2.1). Vartdalsfjorden is around 16 km long, in SW/NE orientation, and 3 km wide, in NW/SE orientation. Vartdalsfjorden stretches from Yksnøya in the southwest to Hjørungneset in the northeast. The average depth is around 300 m, but at the deepest it is 360 m. A sill can be observed between Eiksund and Rjåneset. Vartdalsfjorden is surrounded by high mountains such as Liahornet, Bergehornet and Vardehornet on the south side and Blåtiden on the north side, the mountains has an elevation of 1035, 1024 and 985 m amsl on the south side and 697 amsl on the north side, respectively. Several rivers drains into the fjord, among other Storelva. Storelva drains into Vartdalsfjorden on the southeastern side.
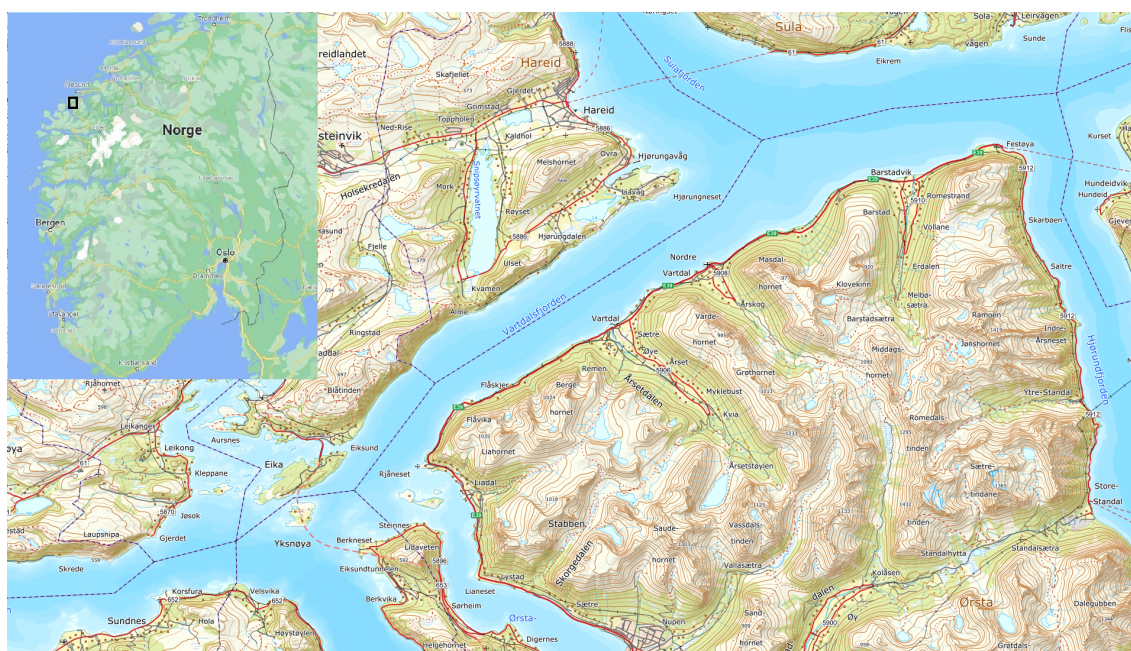
Figure 2.1: Overview maps of the study areas ((Kartverket, 2022); (Google, 2022)).

2.2 Bedrock (tectonic)

The bedrock in the study area consist of granitic gneiss both in the south and north with some lenses of anorthosite, aluminosilicate gneiss and eclogite (Fig. 2.2).
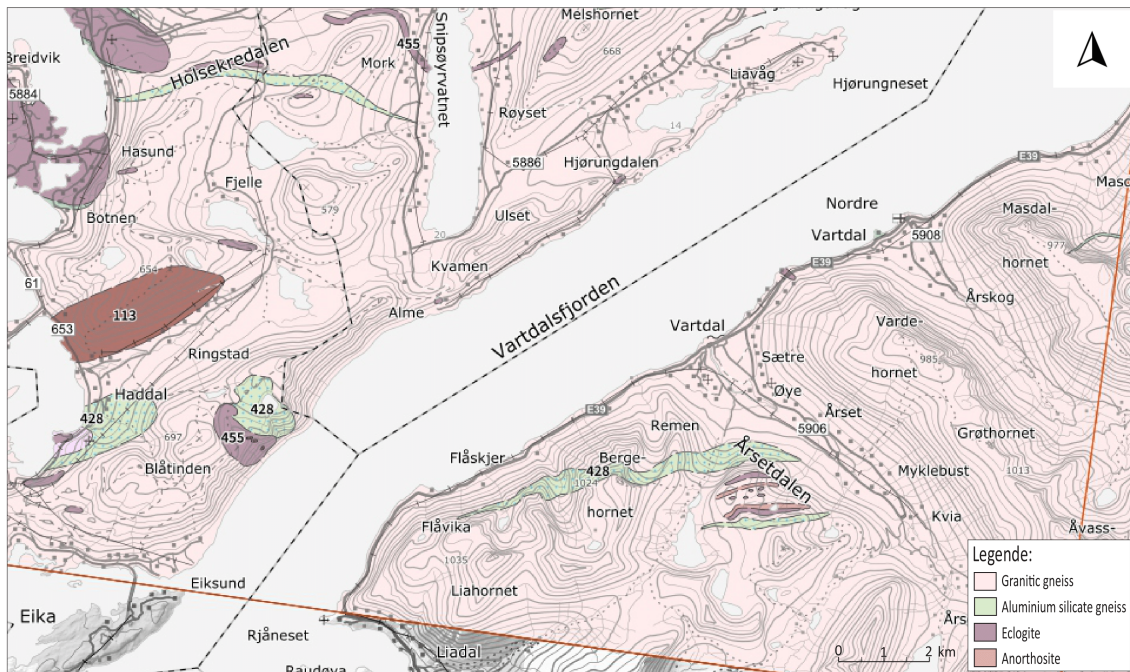
Figure 2.2: Overview map of the bedrock in the study areas. In both south and north (light pink) granitic gneiss (NGU, 2022).

2.3   Deglaciation history

During the Last Glacial Maximum (LGM), defined as the time period from 26.5 ka to 19 ka BP when the global ice sheets reached their maximum volume (Clark et al., 2009), the Scandinavian Ice Sheet covered mainland Norway and merged with the British Ice Sheet (Svendsen et al., 2004). From the Dated-1 time-slice a detailed reconstruction for the Scandinavian ice sheet can be observed. During the LGM the front of the ice sheet terminated at the Egga edge (Fig. 2.4) (Hughes et al., 2016).

An extensive deglaciation took place at around 15 ^{14}C ka BP on the mid and southern Norwegian Shelf, which encompassed the deglaciation of the Norwegian Channel and the end of the Norwegian Channel Ice Stream (NCIS) activity (Fig 2.3A). As a consequence of the end of the NCIS the northward ice movement on the Måløy Plateau could not be sustained due to it being controlled by NCIS. This indicates open water on the Måløy Plateau, since the area of the Måløy Plateau was deglaciated simultaneously with the cessation of the end of the NCIS. From the available data a minimum retreat distance of approximately 30 km from the edge of Måløy Plateau (Fig. 2.3B) as evidenced by the buried iceberg scour marks (Nygård et al., 2004).

The Bremanger Event has been dated to <15-13.3 ^{14}C ka BP. After the retreat, there were open water on the Måløy Plateau and as the ice advanced during the Bremanger Event (Fig. 2.3C), and the Bremnanger Moriane was deposited. The glacier which deposited the Bremanger Moraine could have been sensitive to sea level changes, and the two factors which influenced the sea level during this period was global sea level and glacial isostasy. From 15 until 13 ^{14}C BP the sea level rose around 3-4 mm/year, but after around 13 ^{14}C the sea level rose about 16.7 mm/year which might have caused the retreat of the glacier (Nygård et al., 2004).

During the period of Allerød-Younger Dryas the Scandinavian Ice Sheet had a major regrowth. The Younger Dryas moraine can be more or less continuously mapped around the entire ice sheet. But radiocarbon datings from the moraine are sparse and some parts are not dated at all. In western Norway the Herdla-Hardangerfjorden area moraine is well dated and is an exception. There are three reasons for this, 1) several areas which have been over-run by the Younger Dryas glacial re-advance have been dated, 2) The Herdla-Halsnøy Moraine have been accurately dated and 3) a row of undisturbed Allerød-Younger Dryas lacustrine sequences located distal to the moraine indicate that the ice margin did not extend further west. The mapping and dating from the moraine shows that the ice sheet did not advance out to the Sunnmøre area during Younger Dryas (Mangerud et al., 2016).

The Holocene Thermal Maximum was a warm early-Holocene period which has left a clear imprint in paleoclimate records from mid and high northern latitudes. The Holocene Ther-
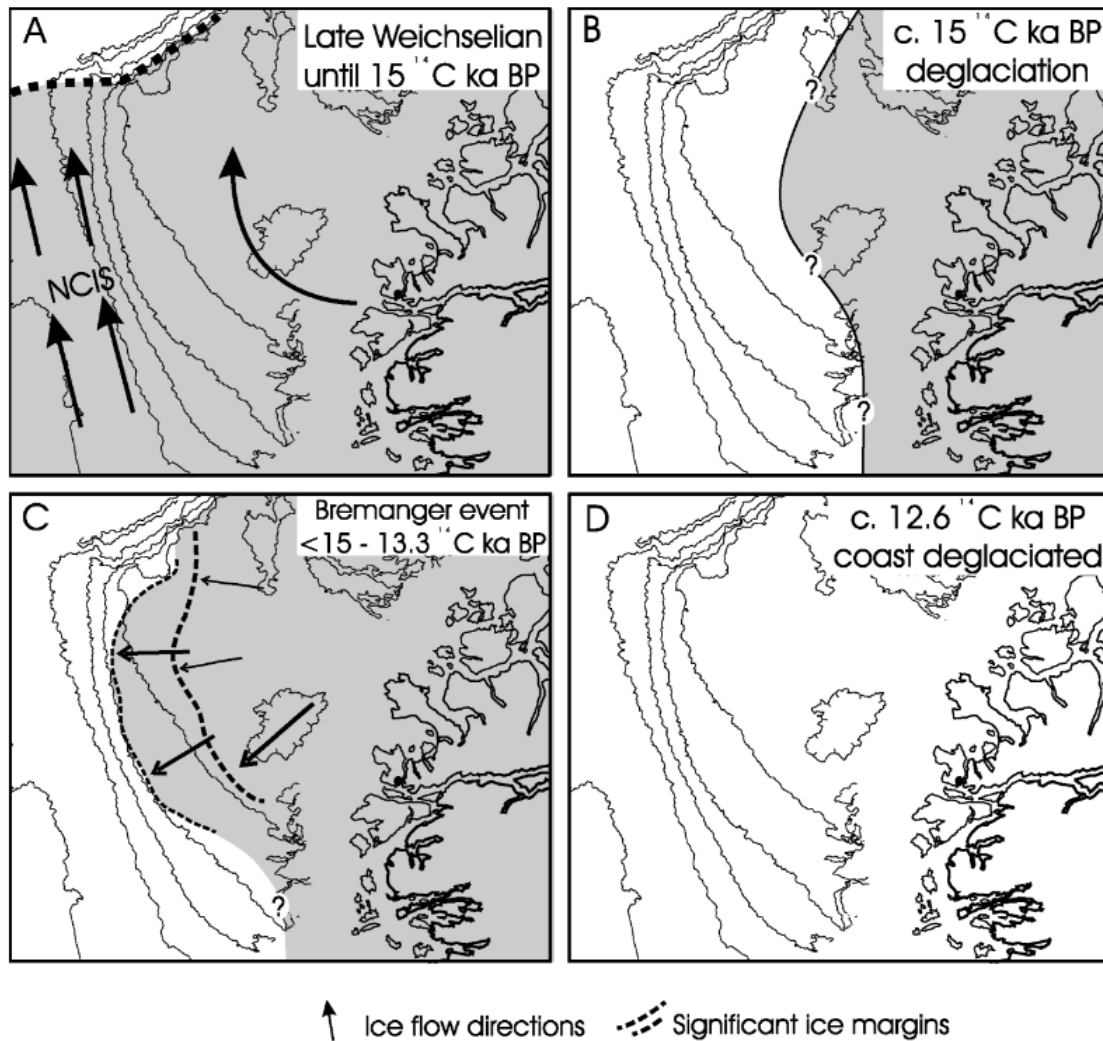
Figure 2.3: A schematic model of the ice configuration at the Måløy Plateau through the last 15 ^{14}C ka BP. This model is based on the morphological features observed (Nygård et al., 2004).

mal Maximum was followed by a mid-Holocene cooling. Both the Holocene Therminal Maximum and the mid-Holocene cooling have been attributed to a variability in solar insulation resulting from orbital forcing (Kjennbakken et al., 2011).

2.4   Sedimentological processes and deposits in fjord basins

Fjord basins are effective sediment traps both during a glacial and interglacial stages. The sedimentary deposits are useful to determine where the ice sheets or glaciers terminated at the last advance and for studying climate proxy records. Typically, sediments will start to deposit at the front of the glacier. When the glacier retreats the sedimentation rate will increase where after it will decrease as the glaciers front retreats to a certain distance (Aarseth, 1997).

Here the most common deposits in a fjord stratigraphy will be explain both in lithostratig-
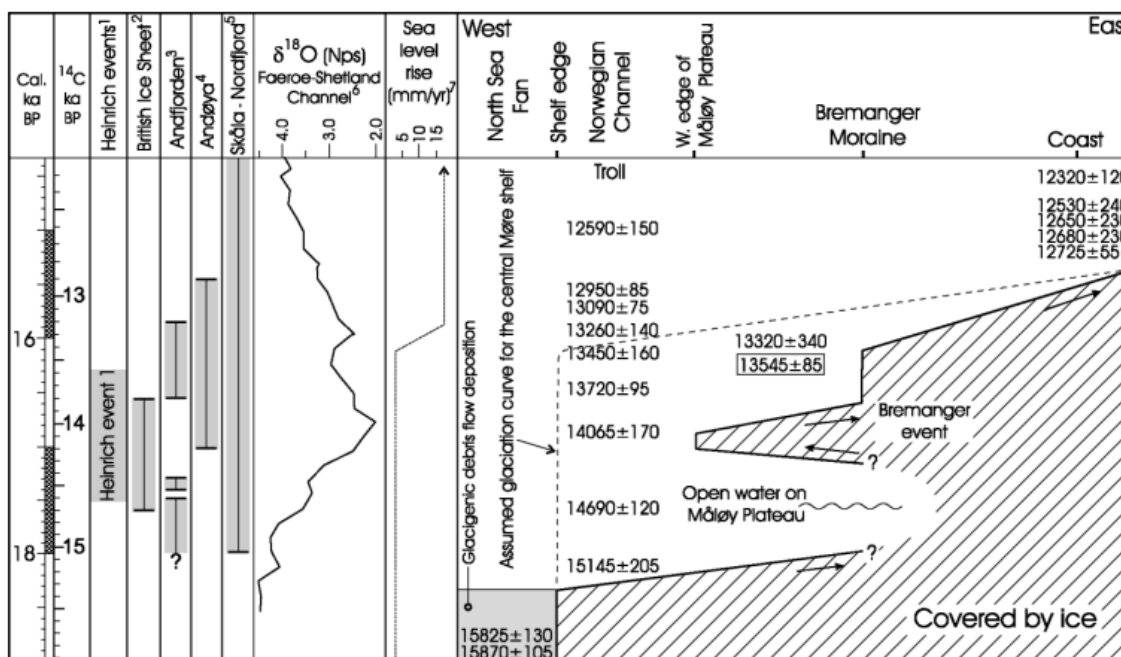
Figure 2.4: A time-distance diagram for the Målǿy Plateau. The date inside the box is from the Trøndelag Shelf and is included because it is assumed to bracket the same glacial event. Climate proxies and periods with deteriorating climatic conditions are also plotted on the same time scale (Nygård et al., 2004).

raphy and seismic character. Hemipelagic layer is a laminated facies and is represented on seismic as parallel to sub-parallel continuous medium to high amplitude reflectors (Hjelstuen et al., 2009). Lack of sorting of the fines indicate that the material is hemipelagic and since the fine grain sizes are not sorted it is not turbidites or bottom current (Lekens et al., 2005).

Submarine slides/slumping in Norwegian fjords is almost always generated in shallow water, either on delta slopes or created by engineering work in the shore zone. The slides are often triggered on shallow water delta slopes with high sedimentation rates. The main reason for submarine mass movements is triggered by liquefaction. On a steep slope a mass movement would be assumed to take the characteristics of a landslide, but on a gentle slope liquefaction could be expected (Aarseth et al., 1989). The seismic facies of underwater slides is an acoustically transparent facies and they typically pinches out towards the flank of the basin. Moreover, slide or slide debrites can also have a chaotic facies (Hjelstuen et al., 2009).

Turbidites can be recognised based on the sorting and mean grain size which distinguish them from plumes. To distinguished between hemipelagic and turbidites the sorting of the fines can be used (Lekens et al., 2005).

Glacioomarine meltwater deposits (plumite) has, like hemipelagic layers, a laminated facies and parallel to sub-parallel mid to high amplitude reflectors on a seismic profile (Hjelstuen et al., 2009). During the terminal phase of Weichselian (last glacial) deep fjord basins acted as an efficient sediment trap. Right in from of the grounding line sedimentation begins at

the base of the glacier. The glaciomarine sediments is mostly deposited in relatively close proximity to the glacier front (Aarseth et al., 1989).

Acoustic basement is the lowest reflector that can be seen on seismic (Peacock and Banks, 2020). This has no clear structural boundaries, and is often recognised as bedrock or moraine in fjords. In the deepest fjords it might be difficult to indicate where the acoustic basement is located. This is due to side-echo from the slopes (steeper than 40 °) (Aarseth, 1997).

2.5   Sea-level changes

During the Ålesund Interstadial the coast of western Norway was free of ice, and subsequently the Scandinavian Ice Sheet covered the area during the Late Weichselian Maximum (Fig. 2.5). It has been suggested that the ice sheet reached the edge of the continental shelf as late as 13 000 BP. If this is the case the deglaciation of the shelf was extremely rapid whereas there is evidence which implies that the outer coastal areas of southern Norway was ice free before 12 500 BP. The dominate mechanism for the ice sheets retreat was calving and it is therefore feasible that the deglaciation occurred so rapidly (Svendsen and Mangerud, 1987).
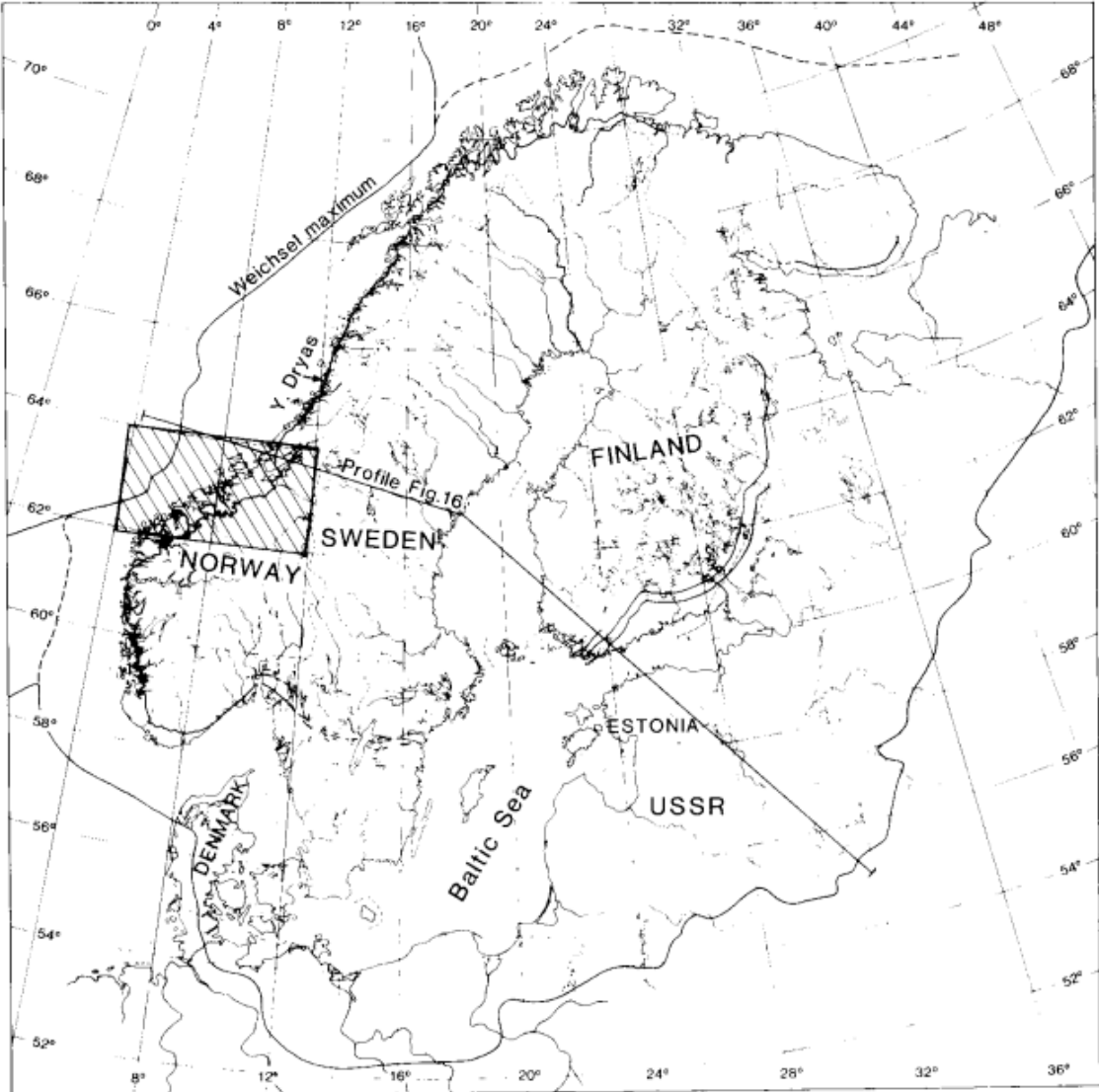
Figure 2.5: The Fennoscandinavian Ice Sheet at the Weichselian maximum illustrated with the black lines, and the dashed lines are alternative locations. The Weichselian maximum (18-20 000 years BP, and the Younger Dryas as presented in Svendsen and Mangerud (1987).
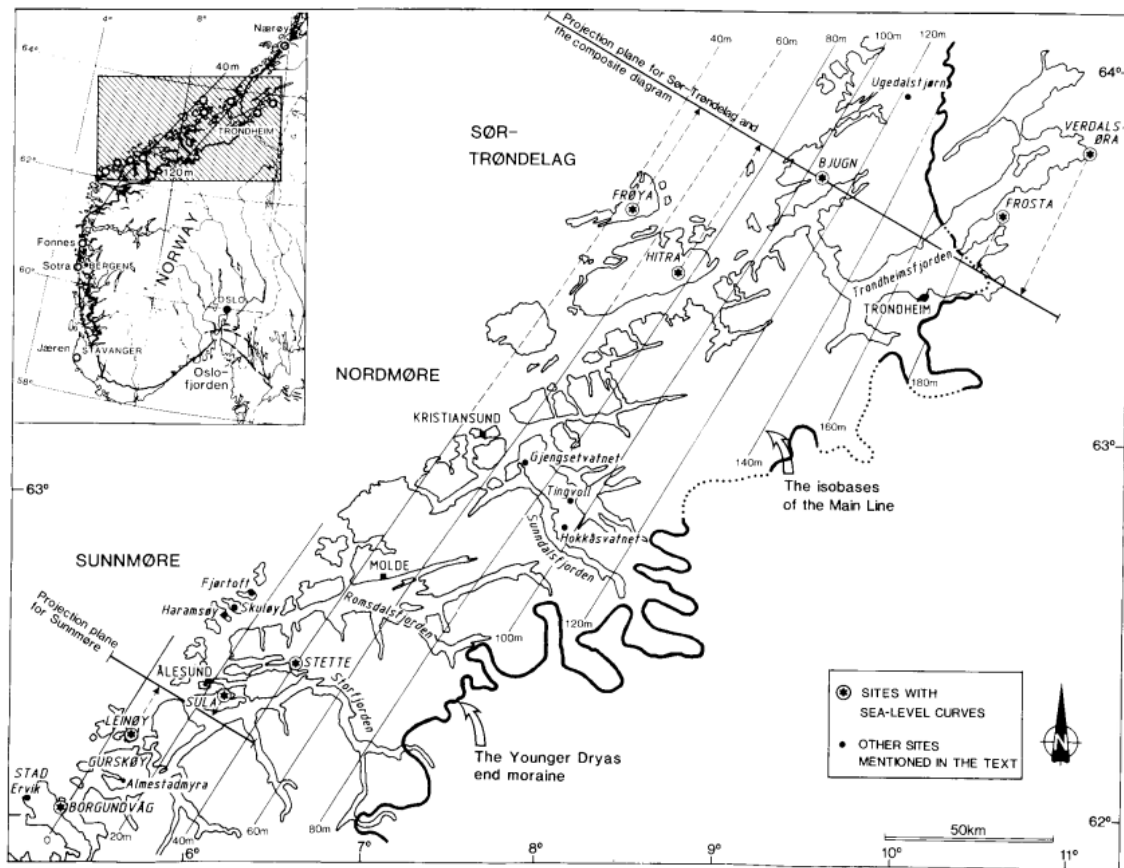
Figure 2.6: Key map of southern Norway, and the main map illustrates the area from Sunnmøre to Sør-Trøndelag. In the lower right corner the projection plane for the sea-level curve for Sunnmøre can be viewed. The Younger Dryas end moraine and the isobases for the Main Line are traced (Svendsen and Mangerud, 1987).

As the ice sheet retreated into the fjords it continued in a rapid pace until an abrupt cooling occurred marking the onset of the Younger Dryas at about 12 000 years BP. During the Younger Dryas the ice sheet front halted or re-advanced in Scandinavia. In Sunnmøre it was probably not a major re-advance, but the detailed history is unknown. The Younger Dryas end moraine as presented in Fig. 2.6 as presented in Svendsen and Mangerud (1987).

2.6 Hydrography and ocean currents

The Norwegian coastline is around 24 000 km from south to north. Along the entire coast the Norwegian current flows. This coast current transports warm water from the Atlantic current and the Baltic ocean current. At Langesundsfjorden the Atlantic and Baltic ocean current meets and continuities northwards as the Norwegian current (Sætre, 2007).

In the spring the salinity can be as low as 25‰ along the coast of Skagerrak, before increasing towards Lindesnes where it can be between $31-34$‰. The cause of this is the supply of saline ocean water from Norwegian current among others. In addition to fresh water supply from rivers along the coast of Norway (Sætre, 2007).

In the fjord the water masses are split into three layers from the bottom; basin water, intermediate layer and brackish water. The basin water is located below the threshold where there is little circulation. Intermediate layer is between the brackish water and the top of threshold. In shallow fjords this layer might be missing. The brackish layer is a mixture between fresh and saline water. The average circulation in the fjord is called estuarine circulation. In the estuarine circulation, saline water is transported inwards in the fjord in the intermediate layer and freshwater streams out of the fjord in the brackish layer (Aksnes et al., 2019).

Important terminology when talking about layers in the water column is thermocline and halocline. Thermocline is a sudden transition in water temperatures in fjords, ocean, and lakes (Saenko et al., 2005). Halocline is a transition between two layers with different salinity. These two factors, temperature and salinity, affect the density of the water and thereby they influence how the water column is split into layers (Schmitz, 2018).

2.7 Biogeochemical reactions and redox zonation in marine sediments

Diagenetic processes in young marine sediments are characterised by decomposition of organic material by different redox reactions and these processes are reflected in the composition of the pore water. (Froelich et al., 1979) developed a simplified model of a pore water profile in marine sediments (Fig. 2.7), which later has been modified with supplementing details and reactions (Schulz and Zabel, 2006). The sequence of redox reactions reflects the biogeochemical and mineralogical zoned sediments and the dominating microbial community growing at a particular depth. In some cases the microbial communities overlap. The idealised pore water profile is based on the dominating dissolved inorganic components and splits the profile into three different zones, oxic zone, suboxic zone and anoxic zone, from the
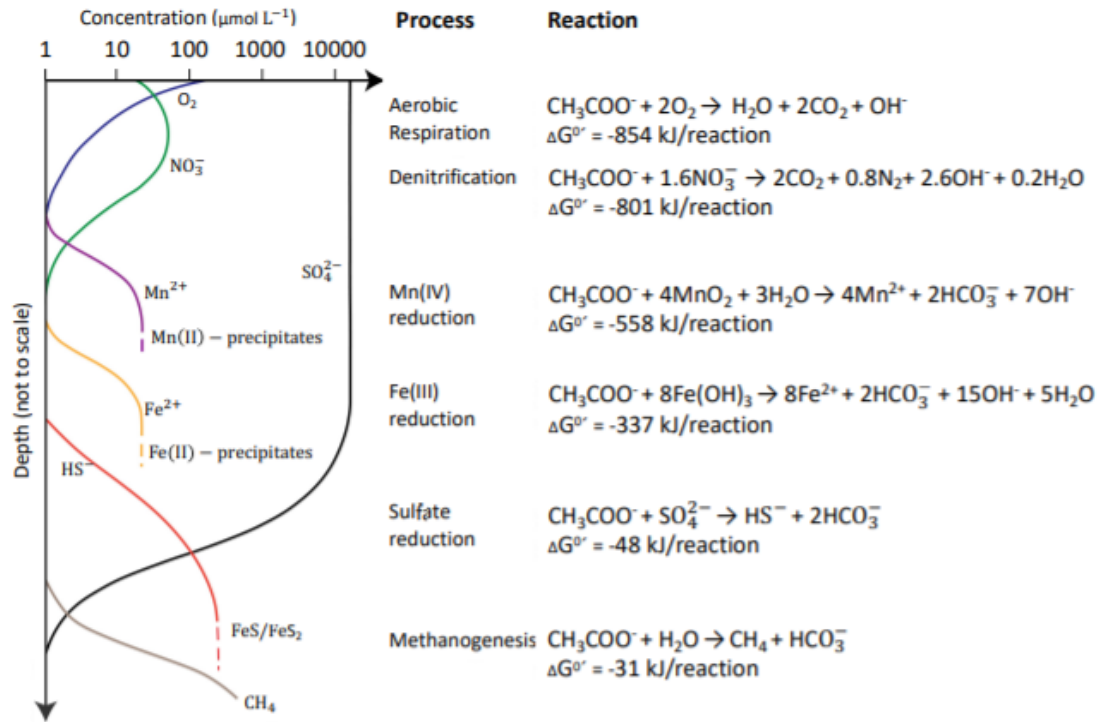
Figure 2.7: Idealised pore water profile in marine sediments based on a dominating electron acceptor with decomposition of organic material. Modified from Froelich et al. (1979) as presented in Konhauser (2007).

seafloor and down through the sediments (Konhauser, 2007). In the oxic zone the concentration of oxygen is gradually decreasing with depth, while the concentration of nitrate (NO_3^-) is increasing simultaneously. The concentration of nitrate is first decreasing in the suboxic zone before dissolved manganese (Mn) and dissolved iron (Fe) successively increases in concentration. The anoxic zone is characterised by a gradually decrease in sulphate (SO_4^{2-}) and a successive increase of hydrogen sulphide (H_2S) followed by methane (CH_4) ((Burdige, 2006); (Konhauser, 2007); (Schulz and Zabel, 2006).

The zonation in the pore water profile is directly linked to microbial oxidation of organic material with reduction of dissolved O_2, NO_3^-, SO_4^{2-} and CO_2 as well as of Mn- and Fe-rich minerals ((Burdige, 2006); (Konhauser, 2007); (Schulz and Zabel, 2006). The microbial redox reactions are occurring in a sequence of available electron acceptor which means that the highest energy is utilised first. The result of these reactions are the characteristic by-products (NH_4, Mn^{2+}, Fe^{2+}, H_2S, CH_4), which can be detected in the pore water ((Burdige, 2006); (Schulz and Zabel, 2006)). In marine sediments manganese and iron reduction plays an important role in the biogeochemical cycle of many elements (Burdige, 2006). Manganese and iron in the redox cycle can lead to precipitation or oxidation of both transitional and heavy metals (Burdige, 2006).

2.8 Pockmarks

The term pockmark is applied to concave, crater-like depressions (King and MacLean, 1970). They are found at the bottom of lakes and the ocean (Kelley et al., 1994), as well as in fjords, eustaries, on the continental rise, continental shelf and continental slopes. In addition, they have been observed in the deep sea (Forwick et al., 2009).

According to (Harrington, 1985) pockmarks are typically between 30-40 m across and 2-3 m deep. Their size ranges from a few meters to several hundred meters in diameter and have a relief of tens of meters (Kelley et al., 1994). They can also be so-called mega pockmarks which can be up to 1.5 km in diameter and exceed a depth of 150 m. Pockmarks can occur both as single and chain units, the chains can be several kilometres long (Forwick et al., 2009).

The classification of pockmarks is based on the morphology, state of development, formation mechanisms and lateral distribution. The controlling factor for lateral distribution is tectonic lineaments, buried channels, underlying permeable bedrocks and lithological boundaries (Forwick et al., 2009).

Pockmarks can vary greatly in shape and size, but some shapes and sizes are common. Therefore, pockmarks have been subdivided into six morphological classes; unit pockmarks, "normal" pockmarks, elongated, "eyed", "strings" of pockmarks and "complex pockmarks" (Hovland et al., 2002), They have three stages of development: new, growing or decaying (Forwick et al., 2009).

Several factors control the lateral distribution of pockmarks for instance underlying permeable bedrock and lithological boundaries, slope failures, and areas of rapid decomposition. Furthermore, they appear in areas affected by up-drift of ice that detached from the subseafloor, decomposition of gas hydrates and where gas is released due to melting permafrost.

In addition, grounded moving icebergs and anthropogenic activities, such as trawling and ships anchoring, might lead to the formation of pockmarks (Forwick et al., 2009).

The most common formation of pockmarks is the seepage of hydrocarbon fluids, which are either biogenic or thermogenic of origin, and/or a release of pore water from the seabed (Roy et al., 2015). The gas can also be from a deep petrogenic source (Harrington, 1985). Further research is needed since the formation of pockmarks and their link to tectonic and glaciological features are not well understood (Roy et al., 2015).

The most recognised theory for pockmark formation today is either through the gas or fluids escaping the sediments (King and MacLean, 1970). However, there are several other formation mechanisms such as actions from above the seabed, biological activity and mechanisms related to the last ice age. From above the seabed there is factors such as meteor impact crater, iceberg drop-stones, and man-made artefacts such as wrecks and bombs. The biological activity includes sub-bottom or bottom-dwelling creatures (Hovland and Judd, 1988).

Whether a pockmark is a geohazard is being debated and this is mainly due to the formation of pockmarks. The formation of pockmarks is dependent on gas pressure which varies greatly. Generally it is agreed that the presence of pockmarks might indicate a hazardous seabed setting (Audsley et al., 2021).

3. Material and methods

3.1 Sampling

Two sediment cores from Vartdalsfjorden were obtained during a cruise in June 2020 with R/V G.O. Sars. Core GS20-229-GC21 (GC21) was taken inside a pockmark structure and was 442 cm long, and GS20-229-GC20 (GC20) was taken outside a pockmark structure with a recovery of 332 cm (Fig. 4.12 and 4.13).

Immediately after recovery the sediment cores were split and samples for analyses of organic and inorganic carbon content, pore fluid geochemistry and microbial community composition were taken. These samples were taken at the depths of 5 cm, 10 cm, and every 10th cm until 50 cm, then at every 25th cm until 100 cm. For the rest of the core, samples were taken every 30th cm (see further details in sections 3.5, 3.6 and 3.7).

3.2 ITRAX XRF core scanner

The ITRAX x-ray fluorescence core scanner was applied to map the bulk element compositional along the entire core stratigraphy. This is a non-destructive method for obtaining data from a core (Rothwell et al., 2015). The cores were scanned with a 500 μm resolution for section 1 and 2 of GC21 and 1mm resolution for section 3 for GC21 and GC20.

ITRAX core scanner has several sensors such as optical-line camera, laser topographic scanner, X-ray line camera to measure the transmitted X-ray and high count-rate XRF detection system. These modern core scanners can analyse sediments at intervals less than a millimetre, which can give insight on a decadal, yearly or even smaller scale. The most common elements to use when reconstructing environmental changes in marine sediments are Ca, Fe, Sr, K and Ti (Rothwell et al., 2015).

The scanner emits X-rays on the core, and this causes emission of electrons from their inner shells by filling the vacancy by secondary electrons produce electro-magnetic waves. The electromagnetic waves are unique for the individual elements. The peaks of the wavelengths

are calculated, and attributed to a specific element which provides a semi-quantitative elemental profile from the core (Emmanouilidis et al., 2020).

3.3   Multi Sensor Core Logger (MSCL)

Multi-sensor-core-logger (MSCL) or multi-sensor-track (MST) is a non-destructive method of measuring the physical properties for a split marine core. The core measurement system consists of a computer who controls the transportation and sensors. The sensors can measure the physical properties such as the P-wave, gamma density and magnetic susceptibility. In this study the MSCL was utilised to measure the magnetic susceptibility and gamma density with a resolution of 200 μm.

3.4   Sedimentological methods

3.4.1   Sedimentological description

A sedimentological description of the cores was made based on among other things stratigraphy, lithology and colour. It is common to start by classifying the colour based on the Munshells (1976) colour code which is split into under-groups depending on the hue.

The colour hue of the sediments can be an indication of which depositional environment, as well as the organic material present. Hemipelagic sediments tends to have a more brownish grey colour due to its higher organic content than glacial deposits, which has a grey colour.

Lithological observations with focus on grain size were performed. At the bottom of both cores clay was observed and moving upwards is silty clay except for two turbidites in both GC21 and GC20. From GC21 four samples were acquired for dating.

3.4.2   Shear strength measurements

Shear strength measurements are taken to study the water content and how compact the sediments are. First the core is stabilised, and then a cone with a certain weight is locked in place by a magnet above the core. By pressing on the release button, the magnet releases and the cone penetrates into the core. The penetration into the core can be read, and by calibrating these numbers from a calibration table a shear strength is given. The numbers from the calibration table are multiplied with the gravitational constant to get the shear strength measurements in kPa (Hansbo, 1957).

Two measurements where taken at every 10 cm from top and down until 330 and 430 for GC20 and GC21, respectively. But for some areas there where a big gap between the two measurements so a third was taken between them, and in some areas samples where taken every 5 cm.

3.4.3 Sediment analysis

Samples were taken from the cores by removing sections of 1 cm of sediments with spatula. These where diluted in water and placed on the bench-top shaker, and thereafter the sediment was sifted in fractions of 150 μM, 125 μM and 63 μM.

3.4.4 Loss of ignition

The total organic carbon (TOC) and total inorganic carbon (TIC) were measured using loss of ignition from both cores. Sediment samples (1 cm^3) from different depths was put into digels, and weighted and then put into the drying cabinet for 12 hours. The dry samples were weighted before and after they were placed in the oven for 1 hour at 550 °C. TOC corresponds to the weight loss. To find TIC the samples were burned at 950 °C for 1 hour and then weighted. Potential errors with this method is other materials than organic and inorganic carbon can evaporate in the oven. Here, an error was made when the sample was reheated to 550 for some time after one hour. Studies of the methods shows a strong correlation between TOC and TIC measurements between loss of ignition and other methods (Dean, 1974). sediment with a low organic content seems to have less inconsistency than sediments with high organic content (Heiri et al., 2001).

3.5 Geochemical and biogeochemical analysis

3.5.1 DNA extraction

Using the FastDNA™ SPINKit for Soil DNA was extracted according to the protocol which is supplied in the kit. Samples were thawed before between 500 - 600 mg of sediment were added to the lysing matrix E tubes along with 978 μL sodium phosphate buffer and 122 μL MT Buffer. This was homogenised in the FastPrep instrument for 2×45 sec at a speed of 5.5 and iced down in between. Then the samples were then centrifuged at 14 000×g for 10 minutes to pellet debris, and transferred to 2 mL microcentrifuge tubes. 250 μL PPS (Protein Precipitation Solution) Was added and the samples were inverted 10 times. They were then

centrifuged at 14000×g for 5 minutes to pellet precipitate, and the supernatant was transferred to a 15 mL microcentrifuge tube.

The Binding Matrix suspension was resuspended, and 1.0 mL was added to the supernatant and added to the 15 mL tube. Then the samples were placed on a rotator for 2 minutes to allow binding of DNA, and to settle for 5 minutes to allow the settling of the silica matrix. 500 μL of supernatant was removed and discarded, and next the Binding Matrix was resuspended. 750 μL of the mixture was transferred to a SPIN filter, and centrifuged for 1 minute at 14000×g. The catch tube was emptied, and this step was repeated once so all the supernatant was utilised.

500 μL SEWS-M was added and gently resuspended to pellet using the force of the liquid from the tip of the pipette. Afterwards, the samples were centrifuged at 14 000×g for 1 minute. Emptying the catch tube and then replaceing it with a new clean catchtube was done before centrifuging the samples dry for 2 minutes at 14 000×g.

The samples were then air dried for 5 minutes at room temperature, before resuspending Binding Matrix with 100 μL of distilled water. To increase yield the samples where incubated at 55°C in a heating block. One last centrifuge at 14 000×g for 1 minute so the DNA was eluded into a clean catch tube, and the SPIN filter was discharged. The DNA is ready for PCR (Polymerase Chain Reaction) and is stored at -20°C until used.

3.5.2   PCR

The PCR was done in triplicates and for all the samples and consisted of two rounds of PCR. PCR was done to amplify the 16S rRNA gene, and the gene was amplified with the 805R (reverse) and 519F (forward) primer. The DNA samples were amplified in triplicates using the two primers mention above. A master mix containing distilled water, Hot Star Mix and two primers were made.

For the first PCR 8,8 μL of distilled water, 10 μ 2x Hot Star Mix, and 2x 1μL of Primers 100 μM. The PCR cycles were 15 min at 95 °C, 30x (30 seconds at 94 °C, 30 seconds at 56 °C, 30 seconds at 72 °C), and 72 °C for 15 min the to 4 °C for ∞. After the first PCR electrophoresis was run on every new step that was completed. The gel contains 1,5 % agarose and is mixed 1x TAE, before the gel the triplicates were pooled. For all the gels electrophoresis was run for 40 minutes at 50V.

Prior to purification of the amplicons AMPure$^{®}$ XP magnetic beads and the pooled PCR product were vortex well, before mixing in a 1:1 ratio. The bead mix solution was vortex for 10 seconds, and then incubated at room temperate for 5 minutes. Next the bead mix solution was placed on a magnet for 5 minutes so the beads got separated from the solu-

tion, and for the rest of the steps the plate was placed on the magnet except when vortexing. Clear solution was aspirated and cleared from the plate, and then 500 μL of 70 % ethanol was dispensed into the tubes and incubated for 1 minute. Next the ethanol was aspirated and discharged without disturbing the beads, and the two last steps were repeated one more time. Removing all the ethanol from the bottom and walls of the micro tubes is important as this may contaminate the residual sample. The plate was placed on the table to air dry for 15 minutes, and afterwards 25 μL of distilled water was added to the microbes, and then the plate was sealed before vortexing for 20 seconds. The bead mix solution was placed on the magnet for 5 minutes so that the beads could separate from the solution. The cleared solution was transferred to clean tubes without disturbing the beads. An electrophoresis was run, and a second PCR was performed.

The second PCR is preformed to add the ION torrent adapters and tags to the amplicons. As for the first PCR a Master Mix was made with distilled water, 2x Hot Star Mix and Rev. Primer μM with 0.3, 12.5 and 0.2 μL, respectively. In each well 13 μL of Master Mix, 10 μL DNA solution and 2 μL f 10μM forward primer was added to each well with 1 tag. This means that a different forward primer was added to each well. The PCR program started with 15 minutes at 95°C to activate the polymerase, followed by 10x (30 seconds at 94°C; 30 seconds at 56°C; 45 seconds at 72°C), and 10 minutes at 72°C then 4°C for ∞.

A second clean-up of the amplicons was performed as in step 2, and then an electrophoresis was run to check that the product was clean of primer clouds and other bands remaining. Last the DNA products where pooled together, and here it is important that there is the same amount of moles of DNA coming from each sample. To find the amount of mole in each sample the Quantus was utilised to measure DNA concentrations.

3.5.3 Pore water samples

Immediately after the sediment cores was on deck the cores were split at pore fluid samples was taken on 5 cm, 10 cm, and every 10th cm until 50 cm, and then every 25th until 100 cm, for the rest of the core samples were taken every 30th cm. Same as for the loss of ignition and microbiology.

Onboard the ship alkalinity and pH from the water samples were measured with a mobile pH-measurement (Metrhon 826) and an autotitrator (Metrohn Titrando). Oxygen was also measured. H_2S was measured using a mobile photospectrometer (YSI 9500). The water samples were split up into smaller samples for further analysis at UoB. Nutrients (ammonium, nitrate, and phosphate) were measured using a photospektometri (Quaatro autoanalyzer, Seal Analytical) and the samples were frozen at -20°C. For analysis of anions (Cl, SO_4, Br)

measures were taken using a ionekromography (Methron) and the samples were stored at 6°C. Zinc acetate (ZnAc) was added to the pore water samples to stop oxidation of liquid sulphide to sulphate. Part of the samples were measured for cations and other elements (Na, Mg, Ca, K, Si among others) using the Inductively Coupled Plasma Optical Emission Spectrometeri (ICP-OES, Thermo, Scientific iCAP 7600). The samples were then was transferred to acid washed HDPE flasks and it was added nitric acid at 3%, before being stored at 6 °C.

3.6 Bathymetric data

Bathymetric maps from Høydedata was utilised to study the pockmarks. The Batymetri Søre Sunnmøre 2017 dataset with a resolution of 0.25 m from Høydedata was imported into ArcGIS.

In ArcGIS pro the dataset was first run through the "Batch Convert LAS" then "Create LAS Dataset" and last "LAS Dataset to Raster". Then the "HillShade" tool was utilised to make a 3D bathymetric map of the seafloor. The colour scale was change to get a better shaded relief and the pockmarks and the colour pallet "Black to White" were chosen. The coordinates for the pockmarks was mapped and imported into ArcGIS pro. The pockmarks was measured in the Dybdedata webpage using the measuring tool and the depth and width of the pockmarks was mapped.

3.7 Seismic processing and interpretation

If possible the "Seeded 2D autotracking" function in Petrel was utilised, but double checked, and the manual interpretation was utilised for the areas that could not be interpreted using "Seeded 2D autotracking". The "Seeded 2D autotracking" was mostly utilised in the basins and in the middle of the fjord where the reflectors were strong and continuous, such as the seafloor. On the slopes of the fjords and deeper in the sediments the manual interpretation was utilised, such as for the slopes of the seabed and acoustic basement.

4. Results

4.1 Bathymetry

The Batymetri Søre Sunnmøre 2017 from Høydedata has been utilised to map the bathymetry of the seafloor to get better information about the pockmarks morphological character such as size, volume, and placement. The bathymetric maps show that Vartdalsfjorden has at least 19 pockmarks (Fig. 4.1). The pockmarks in Vartdalsfjorden have ab average of 45 m width and 1-1,2 m depth. The widest pockmark is 81.3 m and 1.4 m deep. The pockmarks are located in the centre of the basin in the fjord (Fig. 4.4).

The pockmarks are located in the central part of the basin in Vartdalsfjorden. The pockmarks are located as single circular pockmarks, but two of them are connected, pockmark 8 and 9.
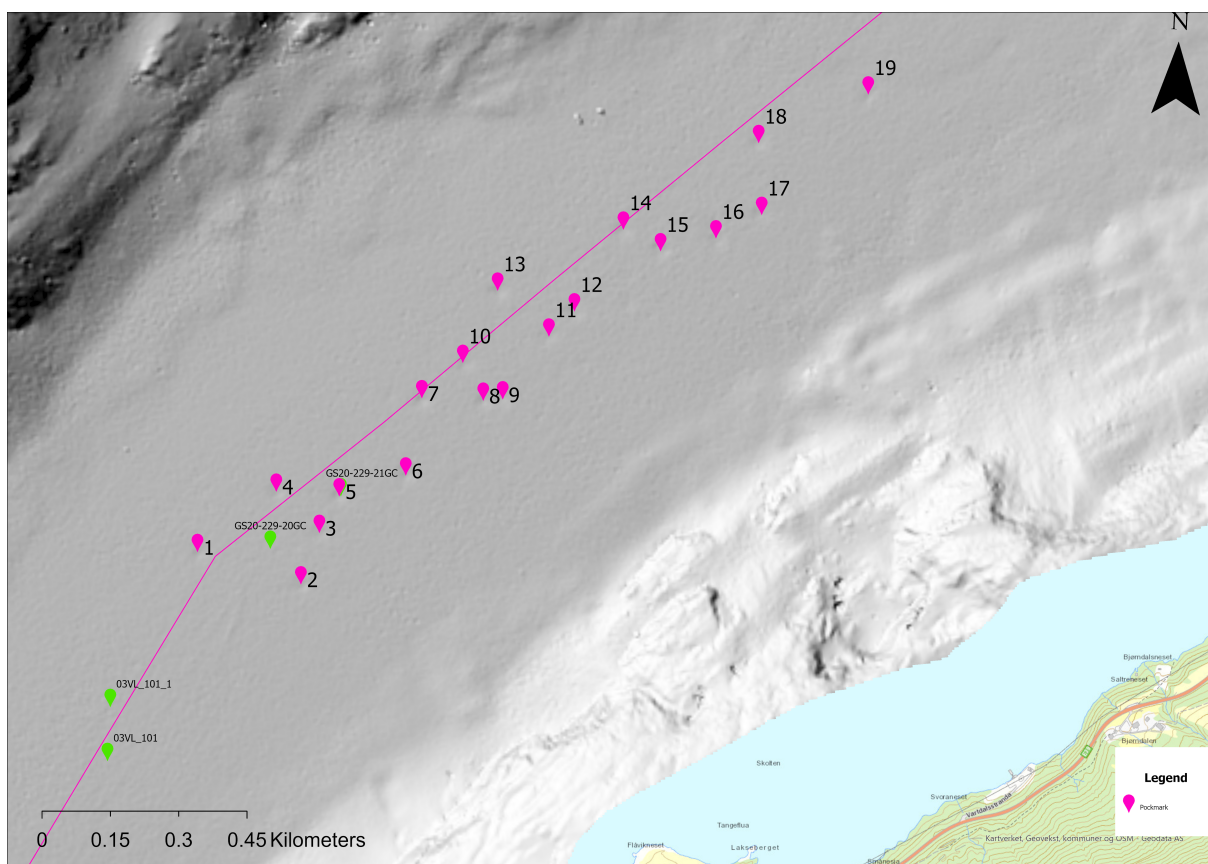
Figure 4.1: In total 19 pockmarks can be observed in Vartdalsfjorden. The pink line represents where line GS20-229-06 is located and the cores can be observed too. GC21 are taken inside pockmark number 5.

Table 4.1: Classification of the seismic facies observed in the study area. The upper facies from I-IIa is shown using figures from the Topas data set collected by the university of Bergen. Whereas the lower facies from IIb and III is shown using figures from the Sparker data set collected by Fugro.

Seismic facies	Description	Interpretation	Figure example
Facies I	Low- to medium-amplitude reflectors Continuous	Hemipelagic	
Facies IIa	Low- to high-amplitude reflectors Chaotic internal structure	Slide and/or slump	
Facies IIb	Low- to high-amplitude reflectors Continuous reflectors	Plumite	
Facies III	Low-amplitude reflectors Semi continuous reflectors	Till	
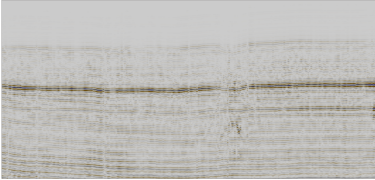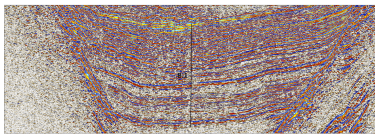
4.2 Seismostratigraphy

In this subchapter the seismostratigraphy of Vartdalsfjorden is presented based on their seismic/facies character (Table 4.1). The sediment stratigraphy of Vartdalsfjorden has been divided into 7 main reflectors (R); reflector R0 (seafloor), R1, R2, R3, RB, RC, RD, and AB (acoustic basement). The stratigraphical units are denoted, SU1 to SU5 where SU1 is youngest and SU5 oldest (Figs. 4.2 and 4.5). Unit SU1, has been further divided into three subunits (Fig. 4.4). The profiles selected for describing the stratigraphy of the Vartdalsfjorden basin are Topas Lines GS20-229-06 and GS20-229-21 (Figs. 4.2 and 4.5), and for the deepest part of the basin Line $H03VL\_01031$ and Line $H030VL\_11022$ from the Fugro data set are chosen (Figs. 4.6 and 4.7).

4.2.1   Unit SU5

The lower boundary of Unit SU5 is defined by the acoustic basement, marked as reflector AB. The unit is characterised by one facies, facies III (Table 4.1), which has low-amplitude reflectors with chaotic internal structure. Some areas have low- to high-amplitude reflectors with no internal structure. The unit is located throughout most of the fjord as it reaches from the middle of the basin and is plastered up onto the sides of the fjord. It has a smooth surface possibly from an ice advanced. Based on the low-amplitude reflectors and chaotic internal structure, combined with the geometry, this unit has been interpreted as till.

4.2.2   Unit SU4

The lower boundary of Unit SU4 is defined by RD (Figs. 4.6) and 4.7). This unit is characterised by a low- to high-amplitude reflectors that is semi-continuous, some areas have a chaotic internal structure (Fig 4.7). The unit has one facies, facies IIb. This unit has been interpreted as melt water plumite deposits based on the acoustic laminated pattern of repeating the low- to high-amplitude which are continuous.

4.2.3   Unit SU3

The lower boundary of Unit SU3 is defined by reflector RC (Figs. 4.6) and 4.7), and R3 (Figs. 4.2 and 4.5). From Fig. 4.2 an area without an interpretation in the middle of the basins can be observed. This is due to Topas data not penetrating far enough into the sediment, and from the seismic it seems like this reflector continues downwards and connects with the RC from the Sparker data, which can be seen on the figure as the orange Xes. This unit consists of three facies. The lower part of the unit is characterised by very low amplitude reflectors with chaotic internal structure, facies IIa. In the middle section the amplitude becomes stronger and generally appear more continuous upwards, facies IIa (Table 4.1), Figs. 4.6, 4.7, 4.2 and 4.5). The upper unit has a low amplitude reflector with chaotic internal structure overlain by medium- to high-amplitude reflectors which are semi-continuous, facies IIb. (Table 4.1). The lower most part of the unit has been interpreted as a slide (Facies IIa). The middle part has been interpreted as plumite deposits based on the continuous reflectors with low- to high-amplitude. The upper part is interpreted to be a result of multiple slumping and/or slide events based on the chaotic internal structure. The boundaries between the slides are characterised by high amplitude reflectors.

4.2.4 Unit SU2

R2 defines the lower boundary of Unit SU2 (Fig 4.4). The seismic unit is characterised by continuous medium- to high-amplitude reflectors, and one facies IIb (Table 4.1). A part of the unit towards the northeast has low- to high-amplitude reflectors and an internal chaotic structure (Fig. 4.4). The part in the northeast has been interpreted as slide or/slump based on the chaotic internal structure, and the main unit has been interpreted as turbidite (hemipelagic) deposits, based on the continuous reflectors and the reflectors amplitude.

4.2.5 Unit SU1

Unit SU1 bracketed between the seafloor reflector R0 and reflector R1 (Fig. 4.2 and 4.5). Here the reflectors are continuous in general of low-amplitude character, facies I (Table 4.1). Two high-amplitude continuous reflectors can be observed, and these two reflectors have been interpreted as turbidite deposits. Based on the continuous reflectors the unit has been interpreted as hemipelagic with turbidite deposits.

Unit SU1.1 Reflector 1.1 defines the lower boundary of subunit SU1.1. The unit is characterised by a continuous low- to medium amplitude reflectors, facies I (Table 4.1, and have been interpreted as hemipelagic deposits.

Unit SU1.2 Reflector 1.2 defines the lower boundary of subunit SU1.2. The seismic facies is characterised by continuous low- to medium amplitude reflectors, and has been interpreted as turbidite deposits.

Unit SU1.3 Reflector 1 defines the lower boundary for this unit. In this subunit four hyperbole can be observed in the stratigraphy and these have a high-amplitude reflectors. This unit has been interpreted as hemipelagic deposits.
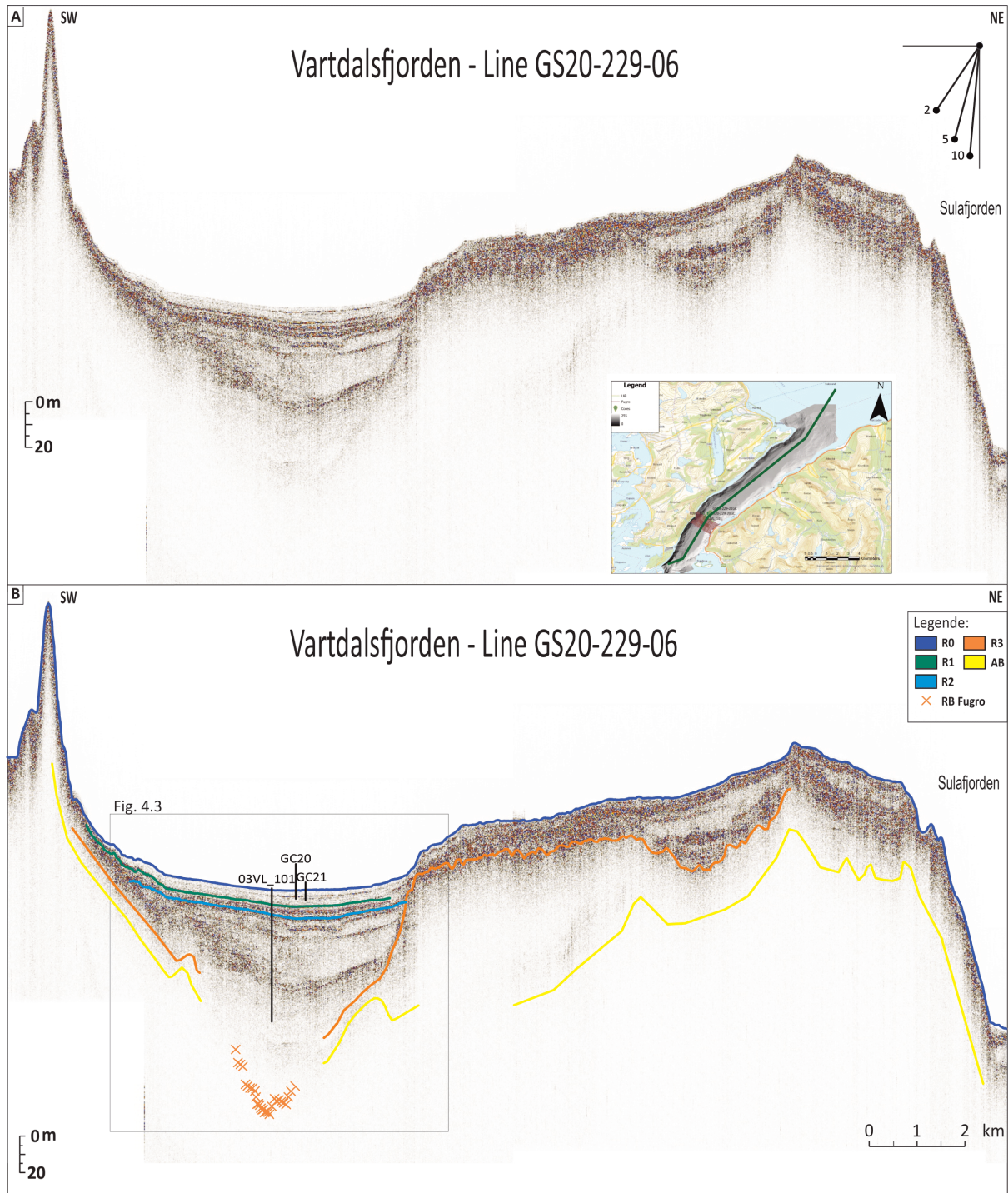
Figure 4.2: Topas line GS20-229-06 A) raw data profile with vertical scale, overview picture and slope rose, and B) interpreted profile.
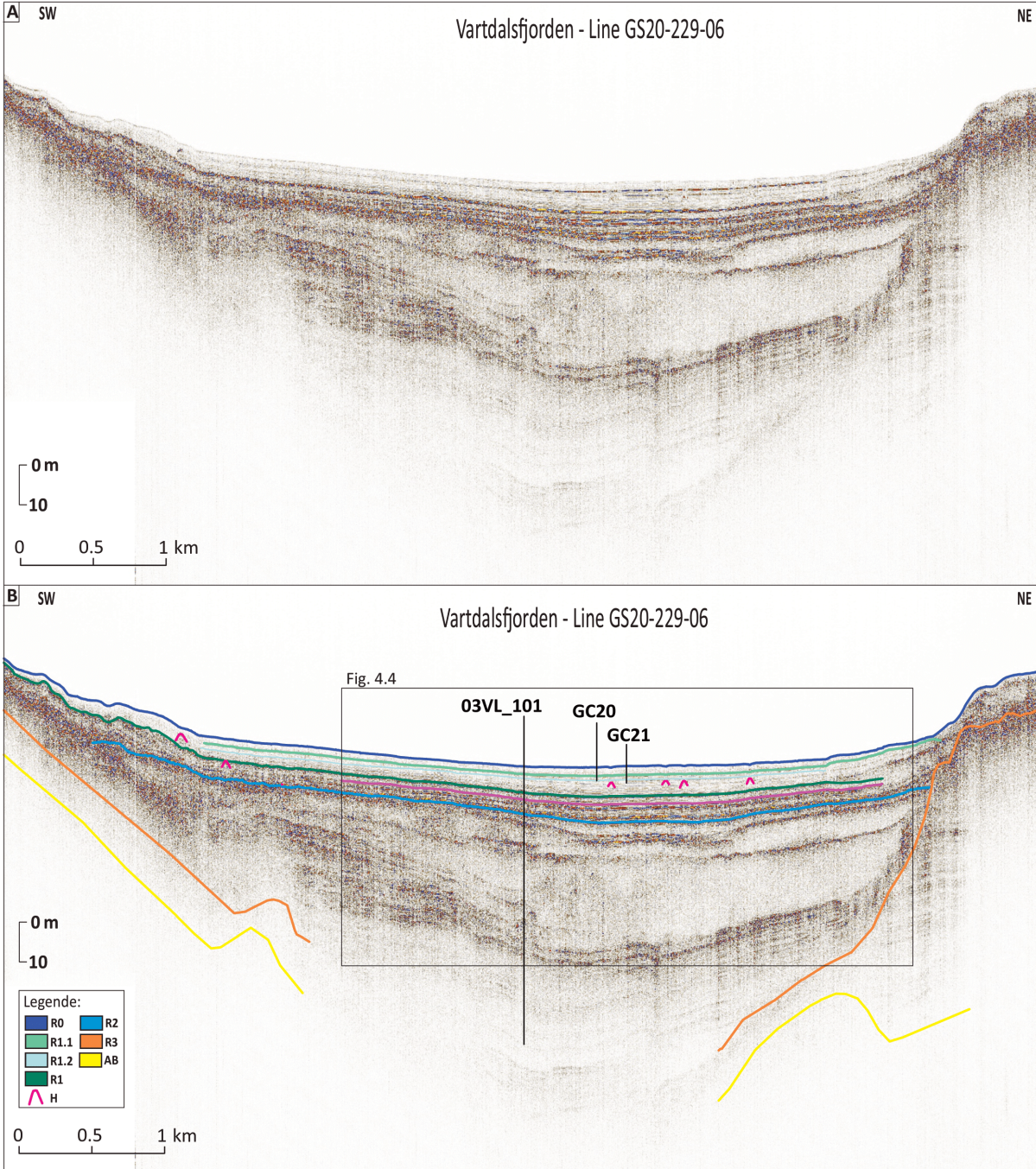
Figure 4.3: A section of Topas line GS20-229-06 A) raw data profile with vertical scale, overview picture and slope rose, and B) interpreted profile.
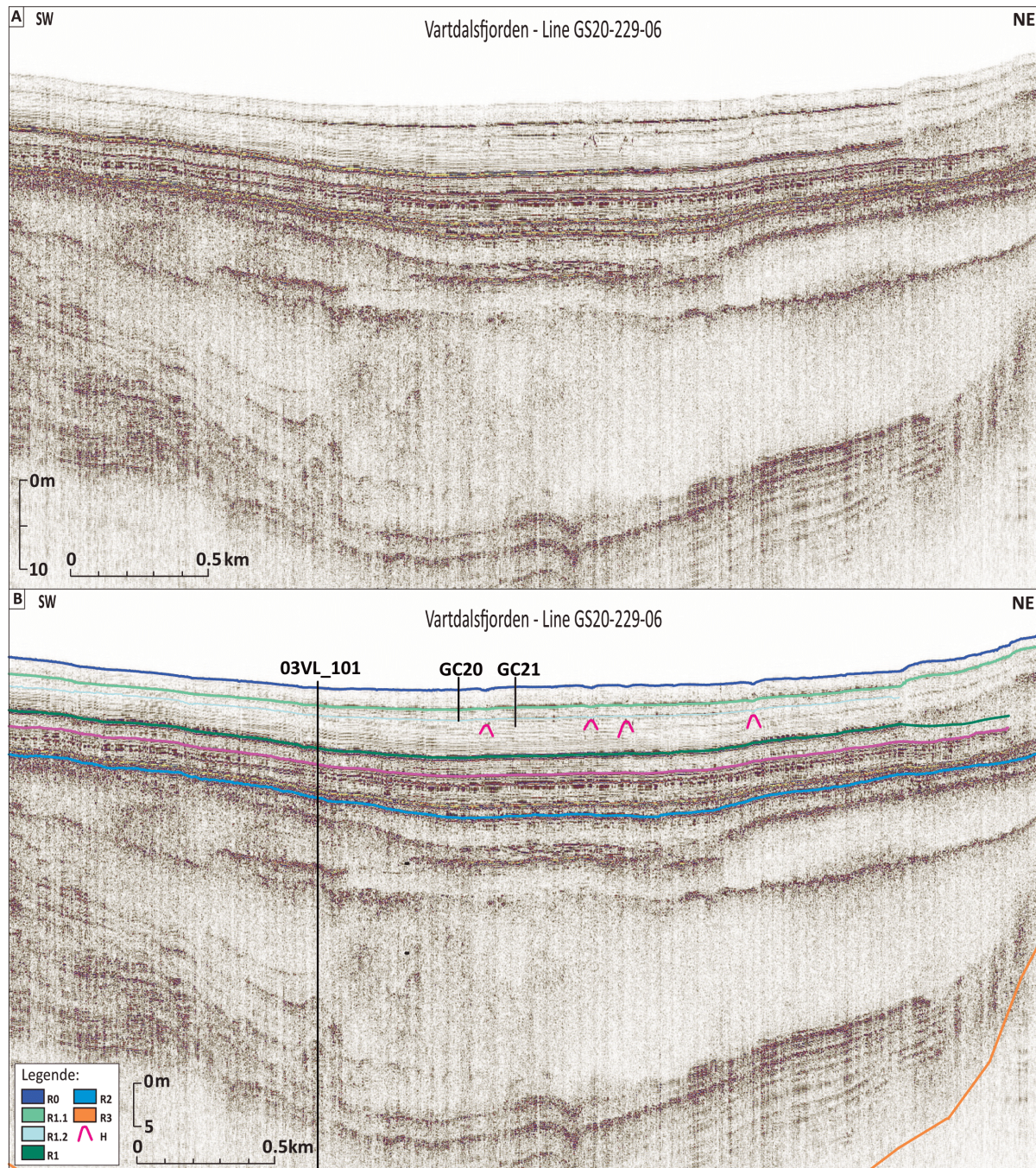
Figure 4.4: Topas line GS20-229-06 A) raw data profile, and B) interpreted profile.
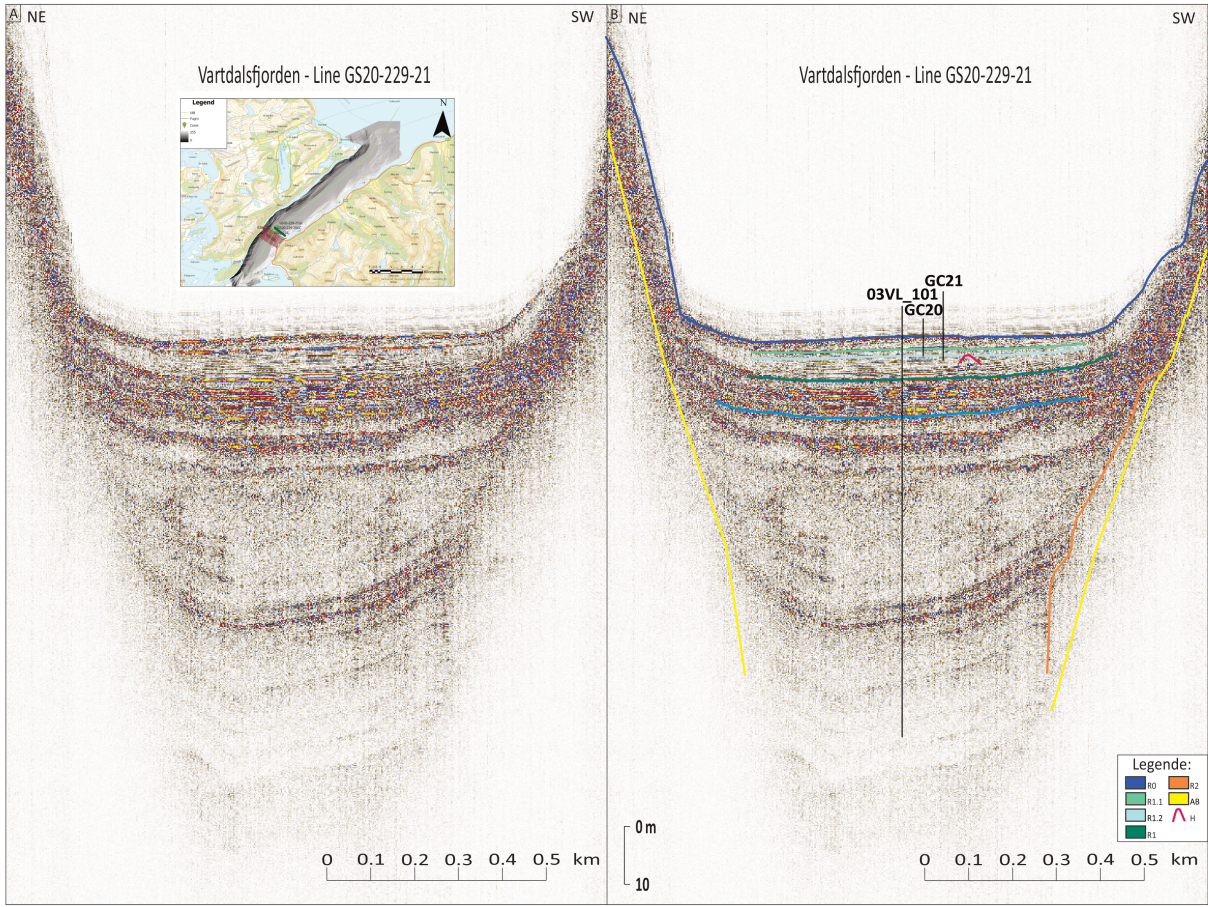
Figure 4.5: Topas line GS20-229-21 A) raw data profile with overveiw photo, and B) interpreted profile with cores.
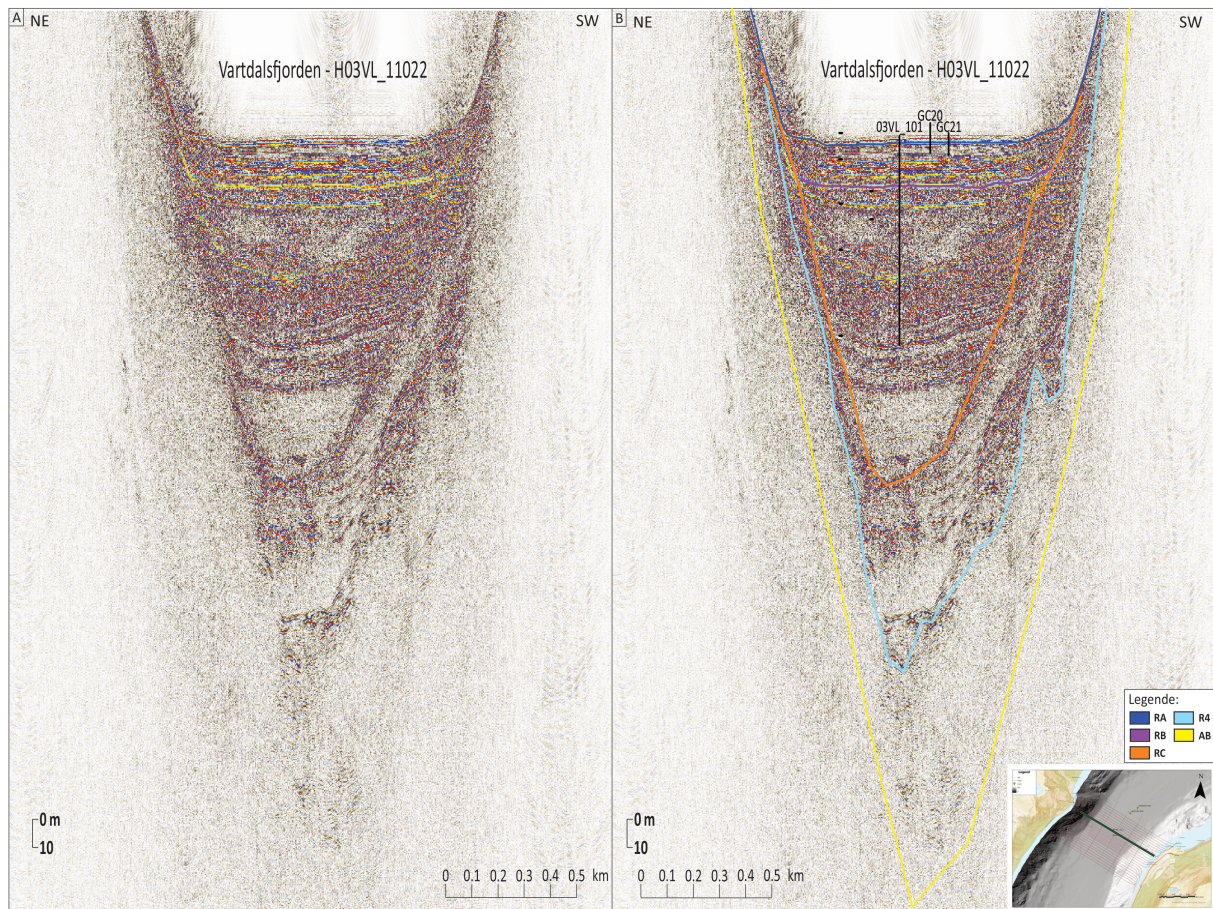
Figure 4.6: Sparker line $H03VL$_11022 A) raw data profile, and B) interpreted profile with overview photo and cores.
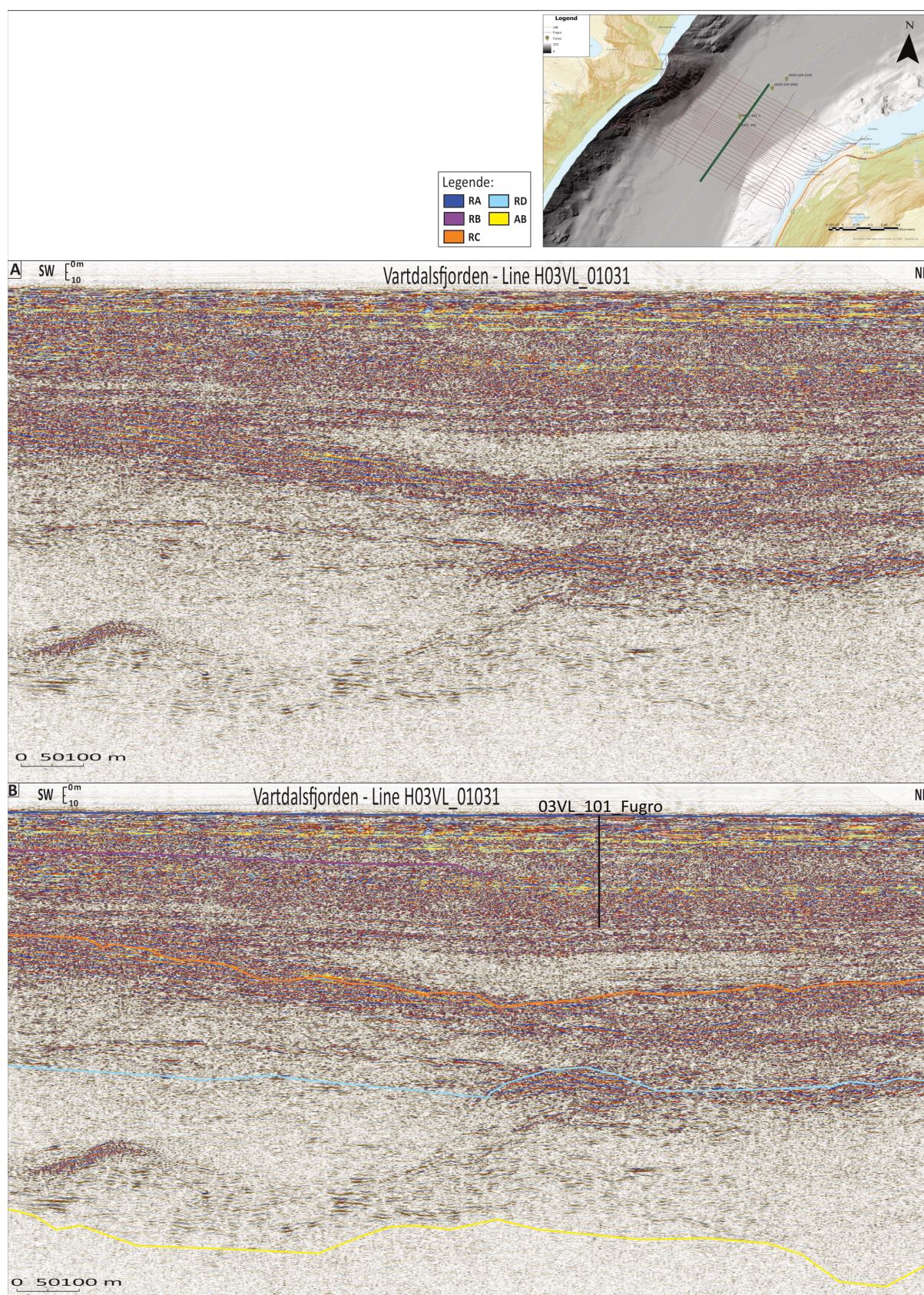
Figure 4.7: Sparker line $H03VL\_01031$ A) raw data profile, and B) interpreted profile with $03VL_101$.
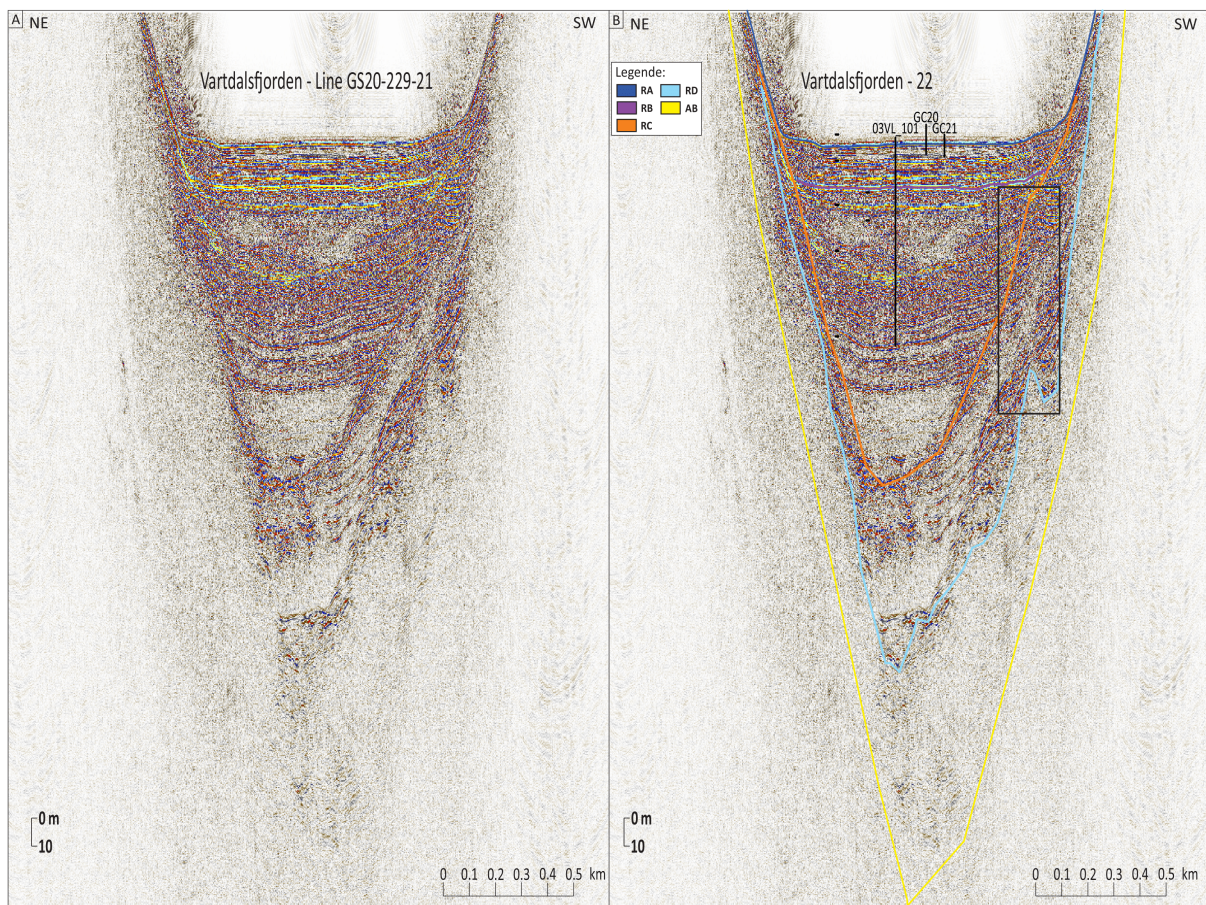
Figure 4.8: Sparker line $H03VL\_01006$ A) raw data profile, and B) interpreted profile.
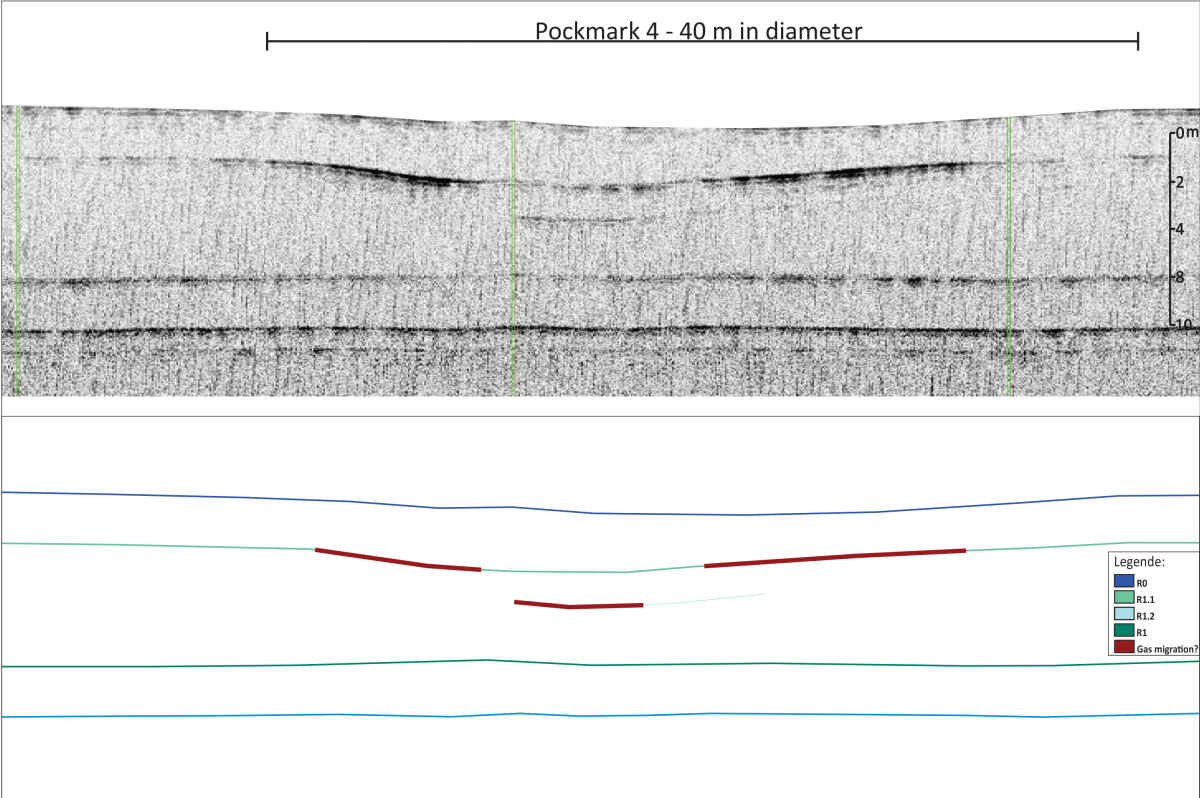
Figure 4.9: Line 4 taken by ROV through pockmarks 4 (Fig. 4.1) with interpretations and a schematic model of the pockmark underneath the profile.

4.3   Core stratigraphy

In this subchapter the core stratigraphy from three cores will be presented and described. The core 03VL_101 is a 71.8 m long drilling core which has been split into 5 units. The results from the analysis of cores GS20-229-20GC and GS20-229-21GC are presented and described (Figs.4.12 and 4.13). The cores have been divided into lithological units based on the visual description, texture, colour, shear strength and grain size analysis. In addition, the logger results from the XRF- and the MSCL core logger (magnetic susceptibility and gamma density) have been used to refine the unit boundaries.

4.3.1   Core 03VL_101

Core 03VL_101 has been divided into 5 informal lithostratigraphic units, denoted Unit 1 to Unit 5.

Lithological unit 5

Unit 5 (39.30 m to 71.88 m): The lower boundary is not visible but is defined by the bottom of the core. This unit is characterised by sandy silty clay. The shear strength decreases up through the unit.

Lithological unit 4

Unit 4 (27.0 m to 39.30 m): The unit is characterised by a dark grey colour, and consists of silty clay. Widely spaced thin to thick layers of sand can be observed. Some gravel/cobbles are spaced in widely to very widely within the layers of sand.

Lithological unit 3

Unit 3 (27.0 m to 13.82 m): This unit is characterised by sandy silty clay, and has a dark grey colour. Closely spaced thin laminae of black clay can be observed with pockets of black matter, which might be organic. Gravel or cobbles can be observed widely to very widely spaced. Also thin to medium layers of sand is observed in this section.

Lithological unit 2

Unit 2 (1.94 m to 13.82 m): This unit is characterised by a dark olive grey colour. Slightly sandy silty clay with thin to medium layers of sand and very widely to widely spaced gravel or cobbles. Traces of shell fragments are observed in this section. The undrained shear strength decreases through the unit.

Lithological unit 1

Unit 1 (0.00 m to 1.94 m): This unit is characterised by a dark greyish brown colour, and the unit consists of silty clay. Traces of shell fragments and a smell of H_2S odour comes from this unit.

4.3.2   Core GS20-229-20GC

Core GS20-229-20GC (341 cm long) has been divided into two informal lithostratigraphic units, denoted Unit 1 and Unit 2. Unit 1 has in addition been divided into 4 subunits (Fig. 4.12).

Lithological unit 2

Unit 2 (341-305 cm): The lower boundary is not visible, but is defined by the bottom of the core. The unit is characterised by fine grained sediments, >99% clay and silt, homogeneous structure and a grey colour (5Y 5/1). No trace of fossils are identified. Based on the visual description and the logged data the sediments in Unit 2 is interpreted to be fine grained glacimarine type of sediments.

Lithological unit 1

Unit 1 (305-0 cm: The lower boundary is defined by a gradual change in colour from light grey to olive grey. The texture is of silty clay and shell fragments and bioturbation can be observed throughout the unit. In this unit there is a general decrease in gamma density from 1.8 g/cc to 1.4 g/cc. Br increases throughout the unit from 700 to 1600 cps, except for an area around 140 cm.

Unit 1d   (305-155 cm): The lower boundary is defined by the gradual transition from the light grey colour to an olive grey colour (5Y 4/2). Texture is of silty clay, and sporadic frag-

ments of shells are observed in this section. Structure is faintly laminated but has been affected by secondary chemical processes.

Unit 1c   (155-130 cm): An erosive contact define the lower boundary lithostratigraphy of the unit. At the base of the unit the grain size is mostly sandy, but the grain size gradually fine upwards to the top where silty clay is dominating. The unit is laminated. Ca/Fe and Br are low in the bottom of the section, but Sr increases. Based on the erosive contact and the fining upwards this the unit has been interpreted as a turbidite deposits.

Unit 1b   (130-20 cm): Dominated by silty clay with an olive grey (5Y 4/2) colour. Fragments of shells and bioturbation can be observed in this unit. TIC and TOC increases from around just above 11 and 4.6 to 14 and 5,2 respectively. TOC has an increase until 40 cm at above 5.4 and decreases thereafter to around 5 at 30 cm before increasing again. The gamma density decreases from 1.6 to 1.4 g/cc in this unit.

Unit 1a   (20-0 cm): The lower boundary is defined by a change in colour from olive grey (5Y 4/2) to very dark grey (5Y 3/1). The texture is silty clay but here quite a bit of bioturbation can be observed. There is pronounced increase in magnetic susceptibility from around 40 to 120 SI 10^{-5}. This unit has been interpreted as hemipelagic sediments.

4.3.3   Core GS20-229-GC21

Core GS20-229-GC21 has been divided into two main informal lithostratigraphic units, denoted 1 and 2. Unit 1 has in addition been divided into 6 subunits (Fig. 4.13). Throughout the entire core there is a general trend in increase of TIC, TOC and gamma density when moving upwards whereas Br decreases.

Lithological unit 2

Unit 2 (440-400 cm) represents the lowermost unit in the core. Due to lack of penetration the lower boundary of this unit is not formally defined. The unit is characterised by a high content of clay and its grey colour (5Y 5/1). A high variation in magnetic susceptibility from 45 SI 10^{-5} to 5 SI 10^{-5}. The shear strength increases through the unit from just above 15 kPa to 40 kPa. Gamma density is generally high 1.9 g/cc and the ratio between Ca/Fe decreases slightly from 0.25 to just above 0.2. There are no traces of shell fragments and fossils in this unit.

Lithological unit 1

Unit 1 (400-0 cm): The lower boundary of this unit is defined by a gradual change in colour from grey to olive grey. Texture is silty clay and bioturbation and shell fragments can be observed throughout the unit. Throughout the unit gamma density and Sr decreases, and Ca/Fe and Br increases.

Unit 1f (400-335 cm) is characterised by its olive grey (5Y 4/2) colour. Variation in shear strength in this unit it varies from around 30 SI 10^{-5} to just under 20 SI 10^{-5} at 380 cm and 350 cm before increasing to 25 SI 10^{-5} at the top. The gamma density has a slight spike at around 375 cm which coincides with an increase in shear strength. Shell fragments and bioturbation can be observed in this unit.

Unit 1e (335-300 cm) is characterised by a sudden change in several parameters at the bottom which defines the lower boundary of this unit. An increase in grain size can be observed in the heat map. Dx(90) and Dx(50) increases from 2.5 and 4 to almost 4 and 5.5 before decreasing again to 2.5 and 4, respectively. In the bottom the grain size is mostly sandy with a gradually fining upwards with silty clay dominating at the top. A spike in gamma density, Sr and the ratio Ca/Fe can be observed between 335 and 325 before they decrease again. The unit has an olive grey colour (5Y 4/2) for the unit.

Unit 1d (300-215 cm): The TIC and TOC increases from the bottom of the section to the top which indicates a increase in organic content. A slight decrease in gamma density can be observed throughout the section, and the shear strength decreases until 285 cm before increasing until 270 and decreasing before increasing slightly. Olive grey (5Y 4/2) is the colour of the section. One spike in shear strength can be observed in the middle of this unit.

Unit 1c (215-145 cm): An erosive contact defines the lower boundary and a sudden change in several parameters. A dip in Ca/Fe, Br and Sr can be observed throughout most of the unit and towards the top it increases. Three spikes can be observed in the shear strength throughout the unit and an increase in gamma density can be observed. From the grain size analysis on the heat map an increase at the bottom and thereafter a decrease supports up under the visual observation that in this unit the sediments is mostly sand at the bottom and moving upwards there is a fining upwards of the sediments with silty clay at the top. The colour of the unit is olive grey (5Y 4/2).

Unit 1b   (145-20 cm): Mostly stable shear strength but a spike around but an spike can be observed at 75 cm. The gamma density has a slight decrease whereas Ca/Fe, Br and Sr increase slightly through the unit. The magnetic susceptibility is stable in most of the unit but it starts increasing towards the top from around 5 10^{-5} just above 20 10^{-5}. Shell fragments and bioturbation can be observed in this unit.

Unit 1a   (20-0 cm): is characterised by a very dark grey (5Y 3/2) and an increase in magnetic susceptibility. The magnetic susceptibility increases from just above 20 to around a 100, which indicates some organic material in the unit. Here, an increase in magnetic susceptibility can be observed from around 20 to 100 SI. The gamma density also increases from the bottom to the top of the unit.
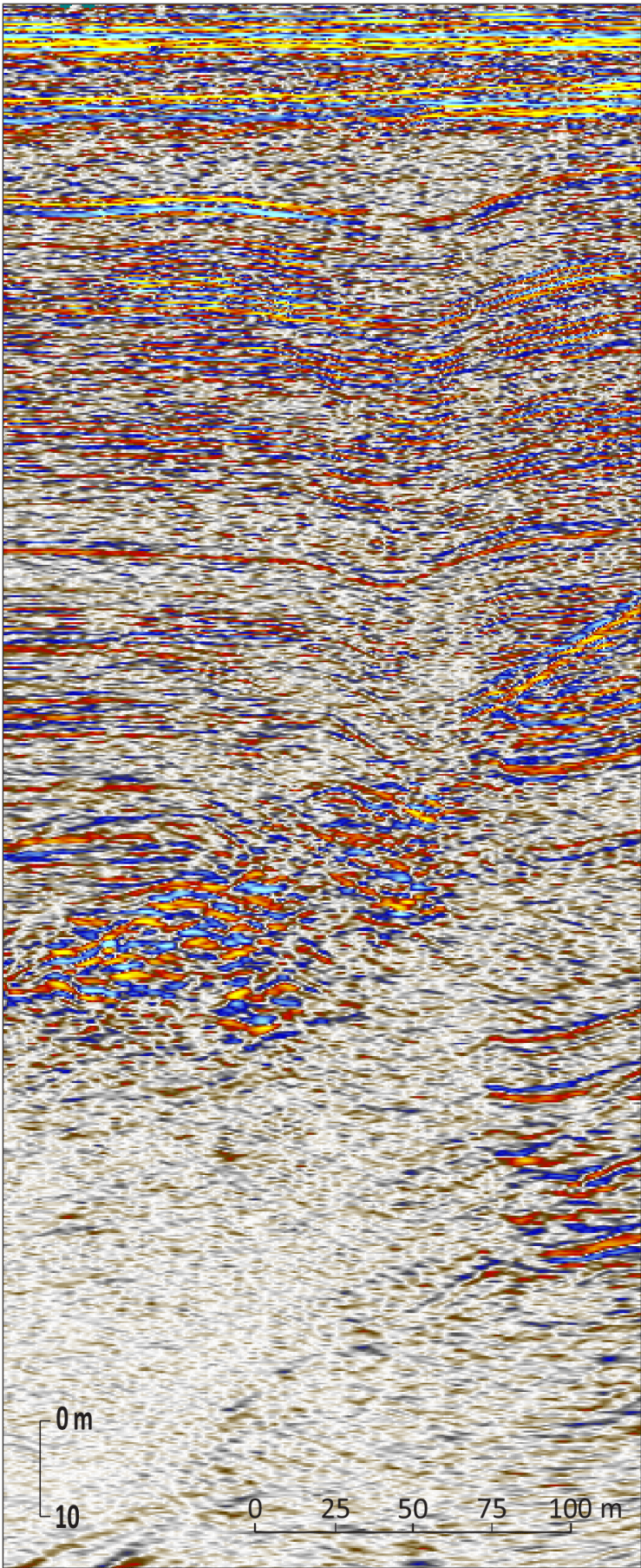
Figure 4.10: A chimney structure can be observed, this is located towards the east of the fjord.
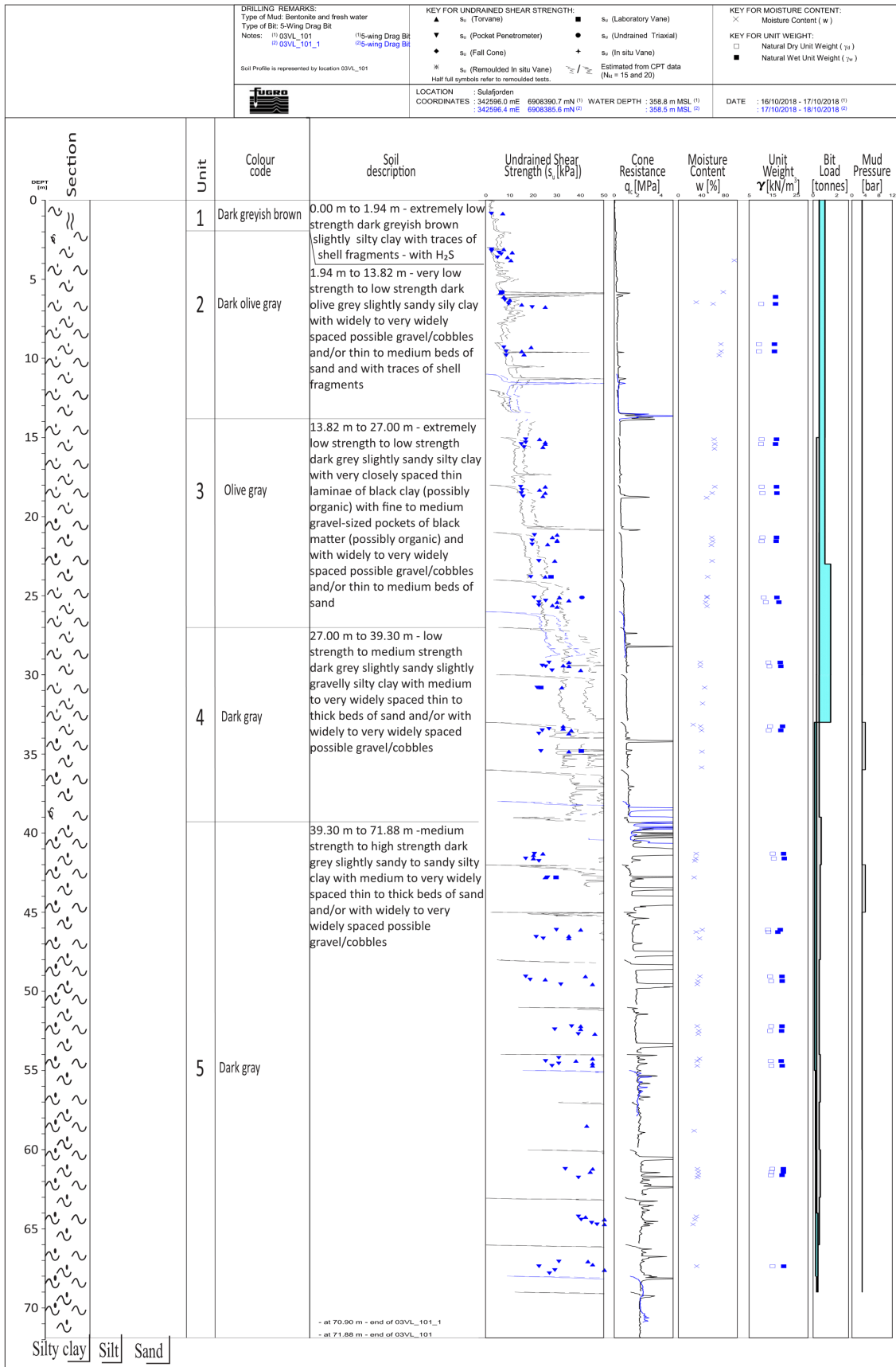
Figure 4.11: Core logs of $03VL\_101$ and $03VL\_101_1$.
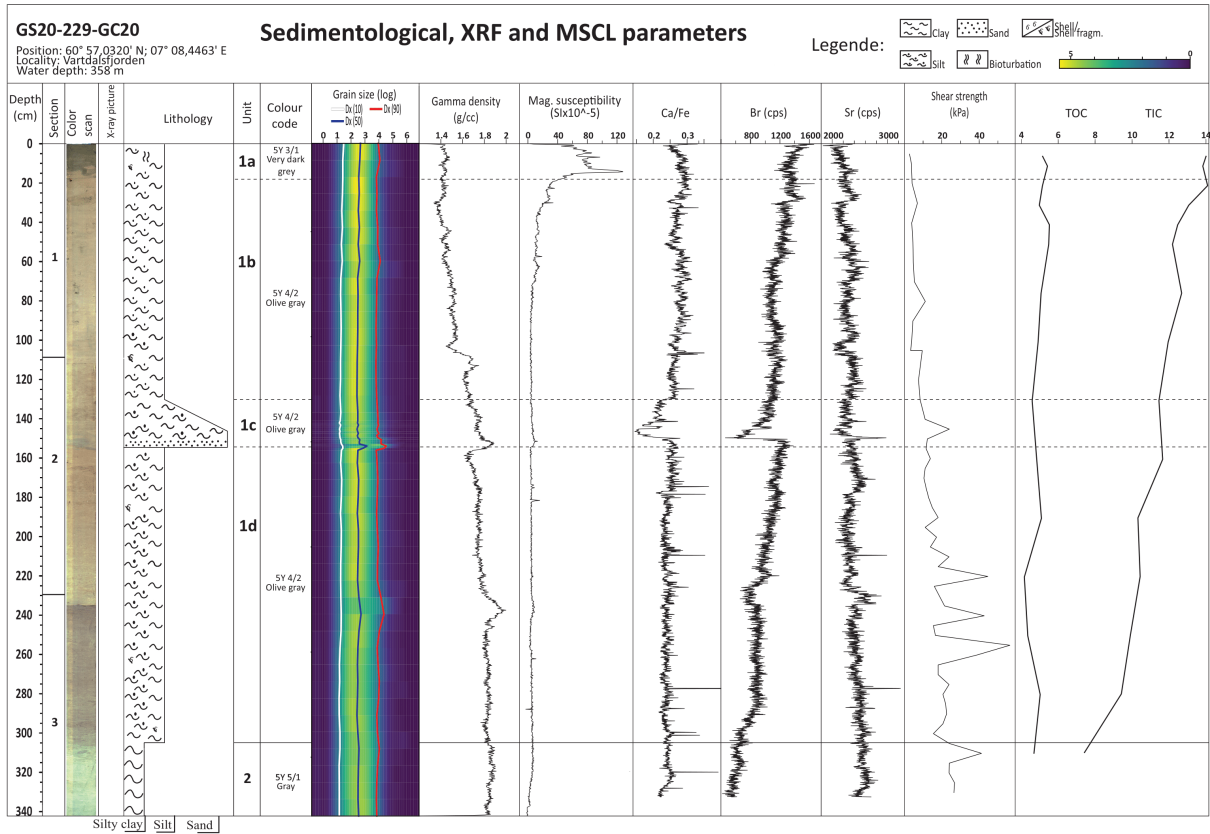
Figure 4.12: Core logs of GS20-229-GC20.
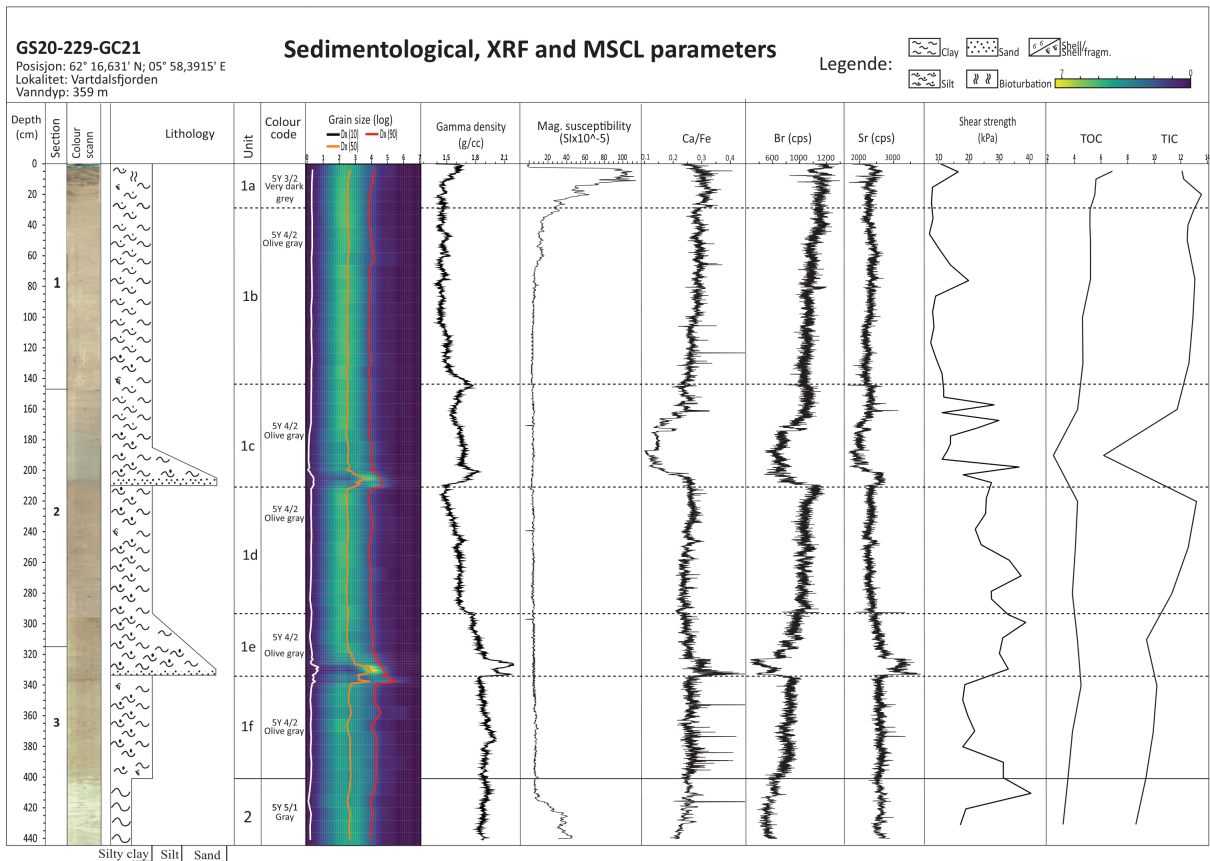
Figure 4.13: Concentration of manganese in GS20-229-GC21.

4.4   Compilation of seismic and core stratigraphy

The core samples retrieved from Vartdalsfjorden by Fugro had a length of over 70 m, and two cores collected by the University of Bergen was over 3 and 4 m. In the cores collected by the University of Bergen, two turbidites can be observed in the upper hemipelagic part of the cores, and glacimarine sediments can be observed in the lower part of the cores.

When compilating and comparing the cores with the seismic from Vartdalsfjorden it is possible to identify several boundaries and facies in both data sets. The top reflector in the seismic profiles is sharp and interpreted to be the seafloor. At a depth of 185-210 cm and 295-332 in GC21 and at a depth of 130-155 in GC20 which coincides pretty well with two reflectors which can be observed in the seismic and are interpreted as 1.1 and 1.2 on Fig. 4.3 and Fig. 4.4. The cores GC20 and GC21 is over 3 and 4 m respectively, and penetrates down into the what has been interpreted as glacimarine sediments.

In the $03VL\_101_1$ the two turbidites can also be observed just below 2 m and just above 3 m as a spike in the shear strength. At 15.6 m on the seismic a high-amplitude continuous reflector, RB, can be observed and this can also be recognised on the core log as a spike in shear strength. The increase in shear strength might indicate a sandy layer in the stratigraphy. Also RC can be recognized on the shear strength measurements as a spike, possibly a sandy layer.

The turbidite at a depth of 295-332 has been interpreted as being connected to the isostatic rebound in Holocene. An alternative interpretation is that the turbidite originated due to the Storegga event, but this seems less possible.

The turbidites that can be observed in GC21 and GC20 at a depth of 130-155 and 185-210, respectively, corresponds to the same reflector due to one core being taken in a pockmarks and one outside a pockmark. These corresponds to the same reflector and have been interpreted as being connected to the isostatic rebound in the Holocene. The bottom of the chronology is defined by reflector 3 in the Fugro data set. R3 is a erosive contact and it is therefore not possible to postulate anything about the seismostratigraphy or core stratigraphy below this reflector due to the hiatus.

4.5   Geochemistry: Pore water profiles

The geochemical analysis of pore water from the cores collected in Vartdalsfjorden is presented in Figs. 4.14 and 4.15. The pH and alkalinity was not measured for GS20-229-20GC, but for GS20-229-21GC the pH was measured at the following depths 5 cm, 10 cm and 20

cm, and alkalinity was measured at 10 cm depth. The pH ranged between 7.48-7.78, and the alkalinity was measured to 2.78 mM.

The concentration of oxygen was below detection at all measured depth (1 cm, 5 cm and 10 cm) on both cores. Nitrate was also below the detection limit in both cores.

Ammonium (NH_4^+) concentration is increasing down through both cores. In GS20-229-20GC it increases from 107 μM to 3167 μM and in GS20-229-21GC from 111 μM to 3216 μM. The concentration is highest in 21GC which is the core taken inside the pockmark. Phosphate (PO_4^{3-} is following the same trend as ammonium in both cores, but it decreases a bit in the bottom of both cores. It increases a bit less in 21GC where it first decreases and then increases again at the bottom.

Manganese (Mn) was detected in a concentration of 23.92 μM in 20GC and 20.75 μM in 21GC. Mn decreases until 160 cm and 340 cm to a concentration of 0.35 μM and nd (not detected), respectively, before it increases towards the bottom to just below 2 μM in both cores.

Iron (Fe) concentration is 3.47 μM and 1.8 μM at a depth of 5 cm for 20GC and 21GC, respectively. There after it decreases to below the detection limit at 10 cm and to the bottom of both cores.

The concentration of sulphate (SO_4^{2-}) decreases through the cores from 27.53 mM and 27.88 mM to 3.90 and 2.64 in 20GC and 21GC, respectively.
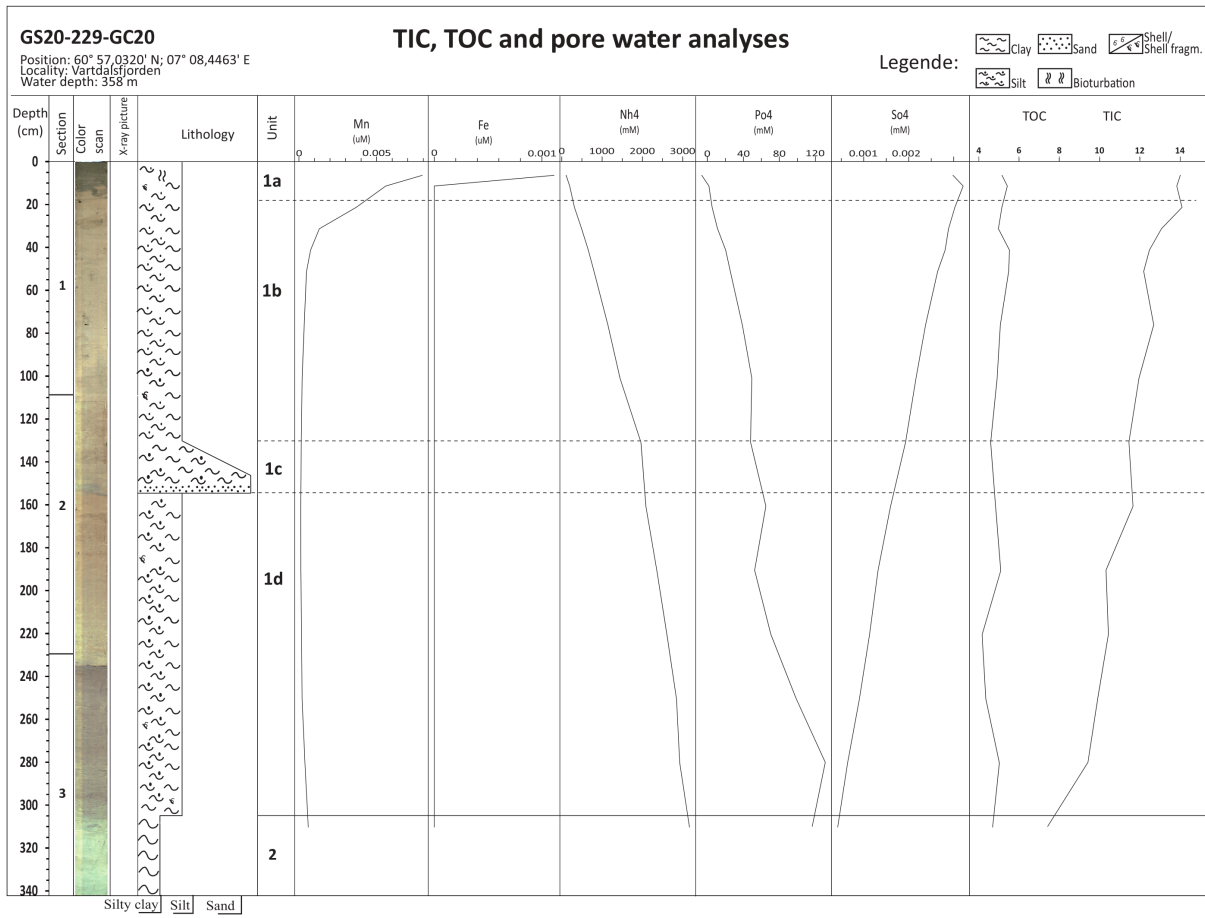
Figure 4.14: Pore water profiles from GS20-229-GC20.
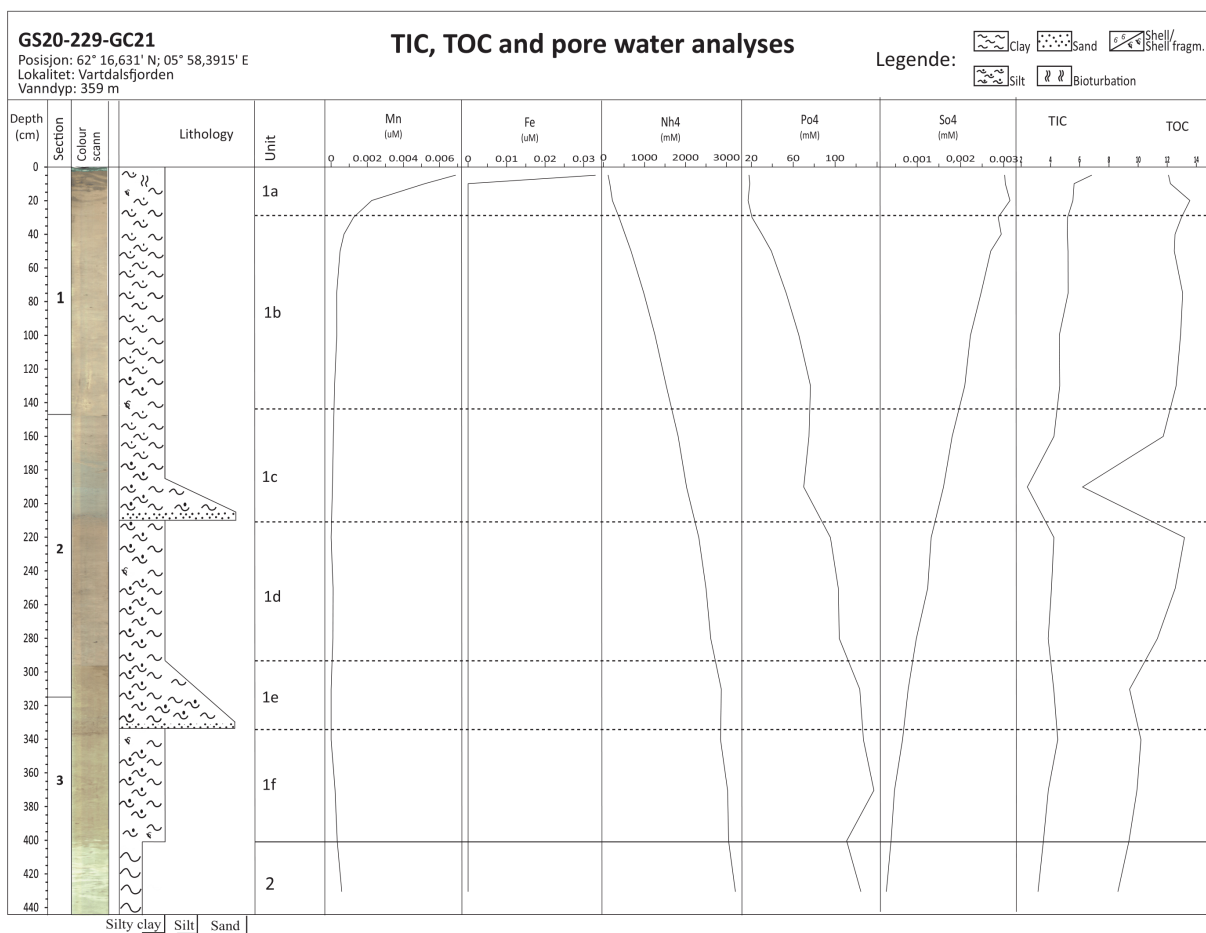
Figure 4.15: Pore water profiles from GS20-229-GC21.

4.6 Geomicrobiology

The geomicrobiology analysis involved a taxonomic profiling of the microbial communities present in the different cores at different depths. Based on the distribution and relative abundance of the different microbial classes (Figs. 4.16, 4.17, 4.18 and 4.19) a PCA plot was created (Fig. 5.6). Assignments (class level) of the microbial samples from the cores collected in Vartdalsfjorden and is presented in Figs. 4.16, 4.17, 4.18 and 4.19. The results shows that the microbial community structure is comparable between the two cores. The variety of microbes observed after running the PCR shows that there is over 10 000 different types of microbes in the marine sediments, divided into over 100 different classes. The classes accounting for less than 1 % were combined in one category called "collected". For GC20 there are 18 microbial classes that accounted for more than 1 % and for GC21 9 classes.
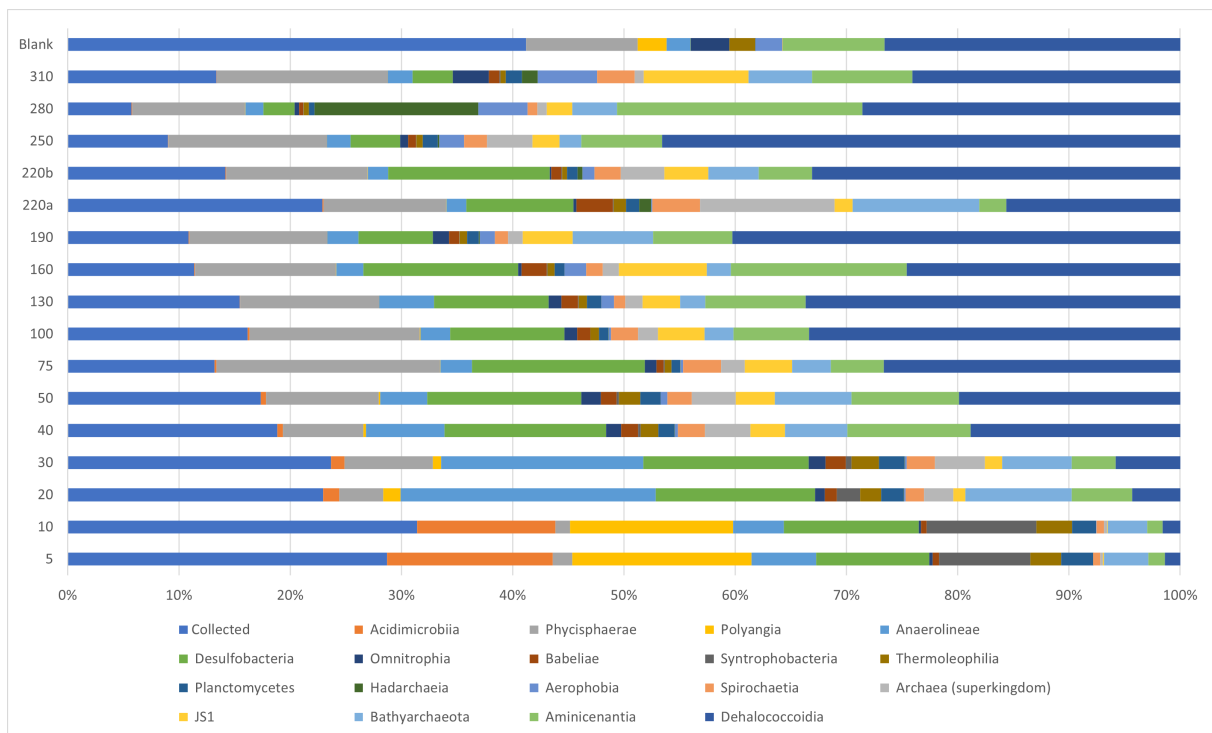
Figure 4.16: Analysis of microbial data from GS20-229-GC20 on class level. The collected category is a collection of all the class that accounts for less than 1 %.
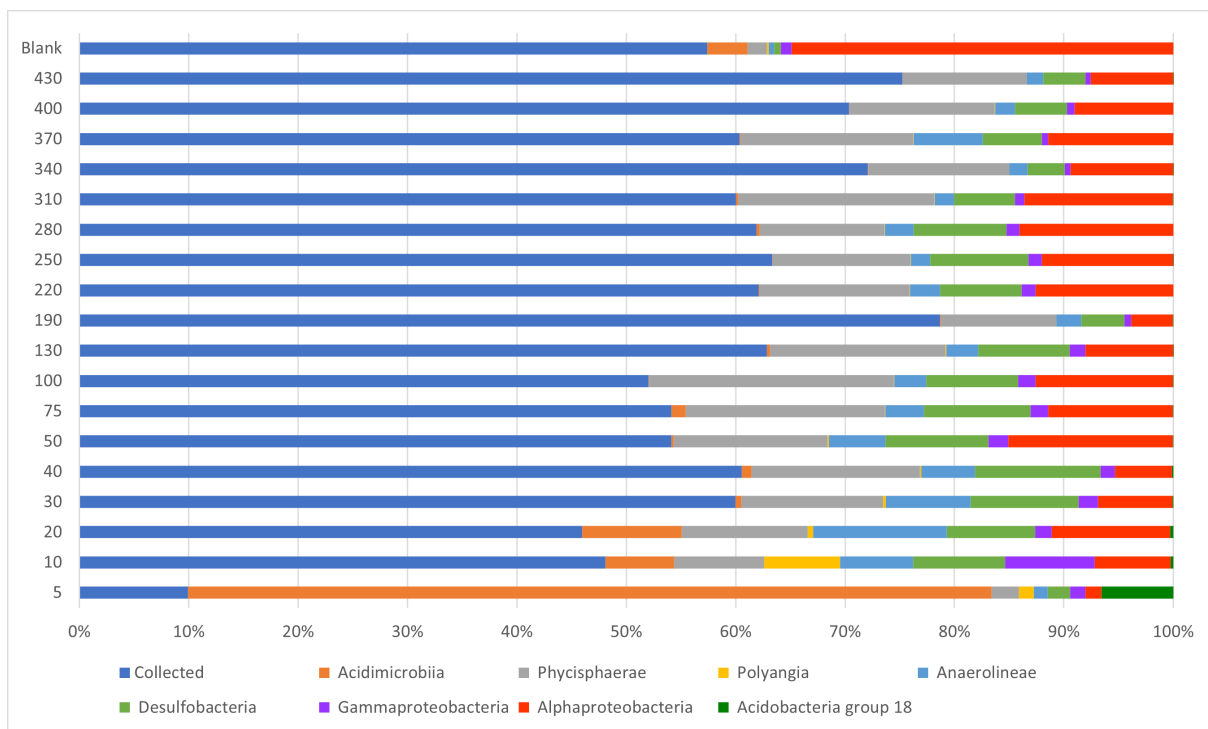
Figure 4.17: Analysis of microbial data from GS20-229-GC21 on class level. The collected category is a collection of all the classes that accounts for less than 1 %.
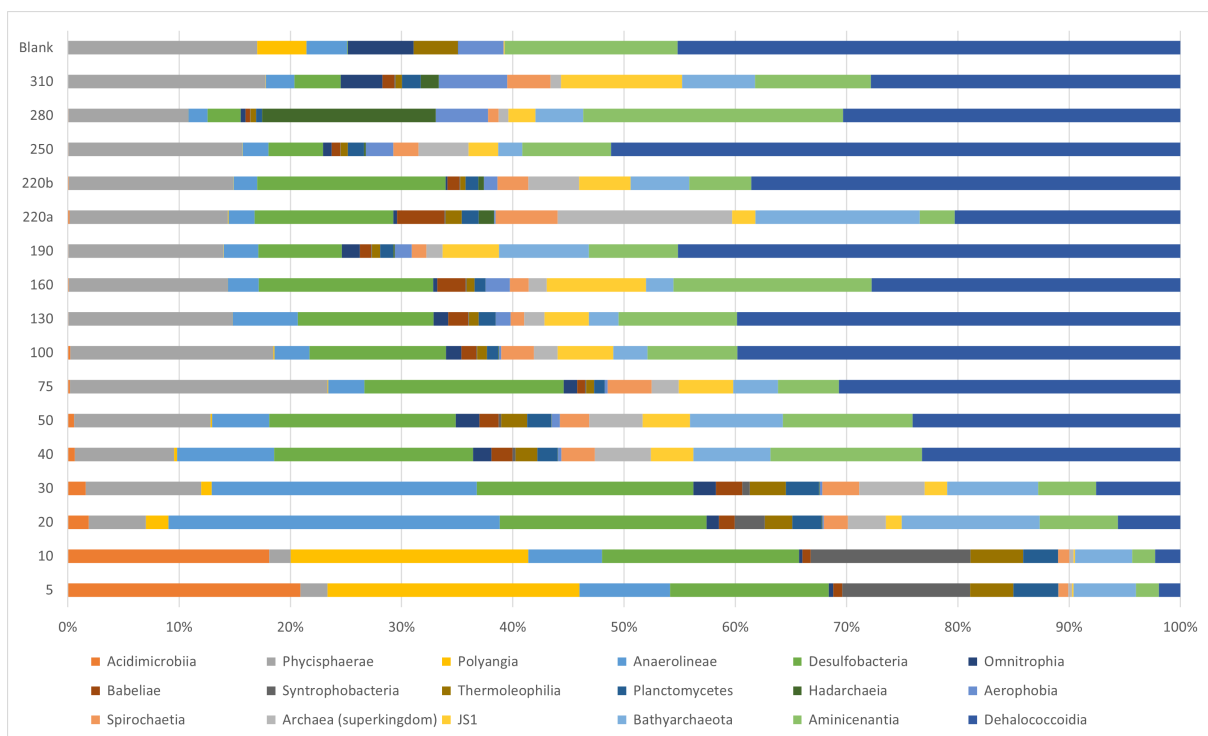
Figure 4.18: Analysis of microbial data from GS20-229-GC21 on class level without collected category.
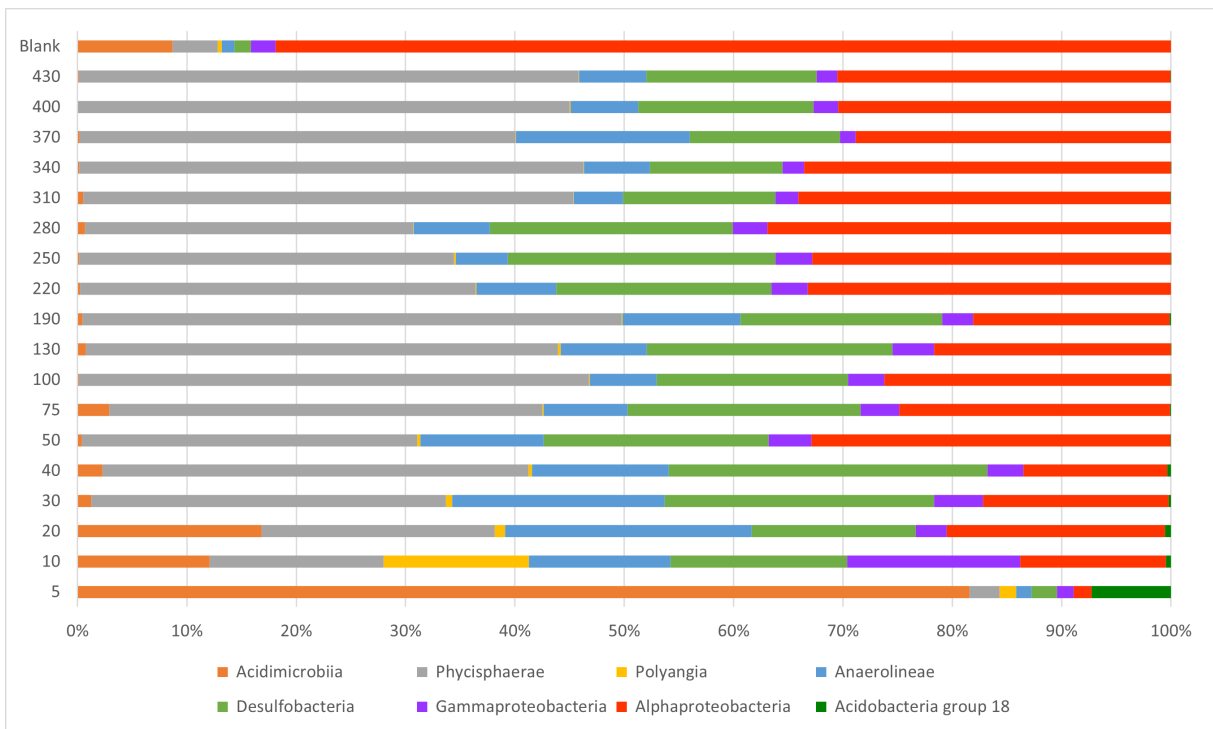
Figure 4.19: Analysis of microbial data from GS20-229-GC21 on class level without the collected category.

4.7 Chronology

In this subchapter the chronology of Vartdalsfjorden is based on the seismic units which is correlated with the chronostratigraphic units. The chronostratigraphy is based on datings and stratigraphic depth from the cores. The dating material is benthic foraminifera and bulk. Two bulk datings were taken from the Fugro core 03VL_101. Here, the upper dating at 41.4-41.6 indicate an older age than the sample at 52.4-54.7 m (Fig. 4.20). Both of these two are bulk datings, and might indicate an older age than they really are. However, when comparing bulk sediments and microfossils radiocarbon dating it is much lower risk for the microfossils to be contaminated by older organic material when it is preformed properly (Hansen et al., 2022). Which in turn will say that the bulk samples are most likely to be indicating an older age. Therefore, it is most likely that the bulk dating at 41.4-41.6 m appear to be older than what is correct. There are several reasons why a dating might show and older age than what is correct such as resedimentation of older sediments or microfossils/foraminifera. The bulk dating is a mean age for all the carbon sources that is present in the sample and will therefore not give an accurate time for the deposition (Strunk et al., 2020).

Table 4.2: Datings from Fugro was utilized for this study. 4 datings from the GC21 was collected. Note that the dating at a depth of 41.4-41.6 m indicate an older age than the one below it and this will reverse the depositional history and has been disregarded. This data is collected from Fugro (2018). Conv. age=Conventional ^{14}C-age (yrs BP), Median age=Median age (cal BP).

Core	Lab. no	Depth (m)	Conv. C-14 age	Median age
03VL_101_1	Beta-527839	9.30-9.55	12 320 ± 40	13 795
03VL_101_1	Beta-527840	25.00-25.45	13 040 ± 40	15 080
03VL_101_1	Beta-528392	41.40-41.60	15 120 ± 50	17 920
03VL_101_1	Beta-530631	52.40-54.70	13 600 ± 80	15 845

Table 4.3: Datings from UoB was utilised for this study. 6 dating from the GS20-229-GC21 was collected). Conventional age = Conventional ^{14}C-age (BP ±1σ), Median age=Median age (cal BP).

Core	Lab. no.	Depth (cm)	Conv. C-14 age	Median age
GS20-229-GC21	LuS 16480	162-163	2354 ± 35	1953
GS20-229-GC21	LuS 16480	211-212	2455 ± 35	2153
GS20-229-GC21	LuS 16477	318.319	3640 ± 35	3583
GS20-229-GC21	LuS 16478	336-337	3800 ± 35	3750
GS20-229-GC21	LuS 16479	399-400	4680 ± 35	4920
GS20-229-GC21	LuS 16480	432-433	6160 ± 35	6541
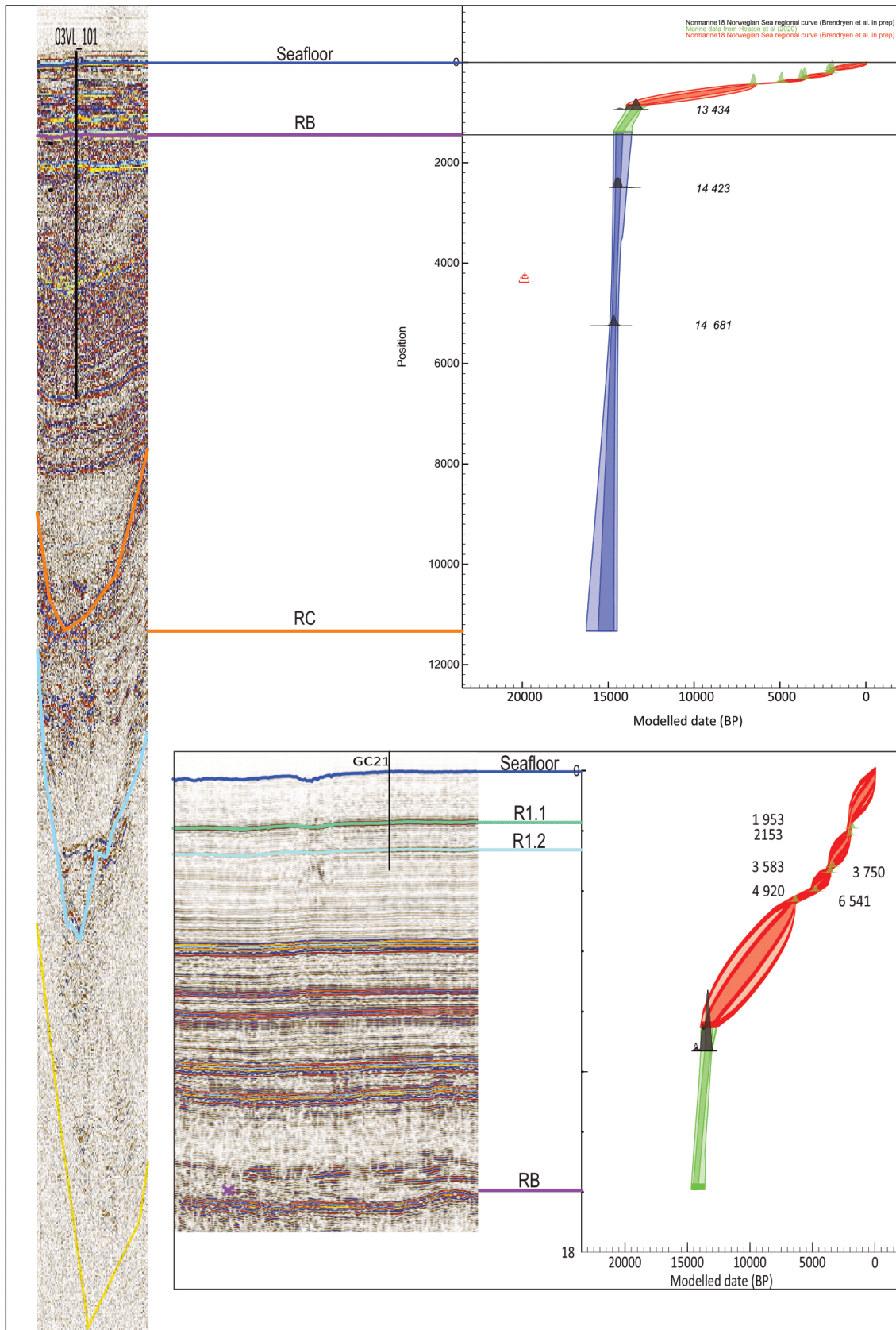
Figure 4.20: A Bayesian deposition model using OxCal 4.4 combining the datings from Tables 4.2 and 4.3 with the core stratigraphy. This was then combined with the seismic profiles from line GS20-229-07 for the upper part of the chronology and line $H03VL\_01031$ chronology from Vartdalsfjorden.

5. Discussion

In this chapter, the results from the bathymetry, seismostratigraphy, core stratigraphy, geo-chemical and geobiological data are discussed in order to increase understanding of the morphology and formation mechanisms for the pockmarks. In addition, to determine an age for the pockmarks. In addition, the sedimentary processes and depositional history of Vartdalsfjorden will be discussed to create a geological framework. Three different hypothe-ses for the formation of pockmarks will be presented and discussed based on the data collected for this study. The discussion chapter will start with an interpretation and correlation between the seismic profiles and chronostratigraphic units, and the depositional processes related to these units. Further, pockmark distribution, pockmark morphology and formation age for the pockmarks be discussed in order to determine whether gas or fluids are present in the sediment stratigraphy. Fluid flow and formation of the pockmarks will be discussed with the focus on determining the most plausible formation mechanism for the pockmarks in Vartdalsfjorden. Last, the biogeochemical processes will be looked at with the intention of determine whether there are gas or fluids escaping the sediments, and what kind of gas or fluid is present in the sediments.

5.1 Chronostratigraphy and depositional history

In this sub-chapter, the chronostratigraphy and depositional history of Vartdalsfjorden is discussed based on a correlation between the seismic profiles and chronostratigraphic units. The chronostratigraphy is based on ten radiocarbon dates (Tables 4.2 and 4.3) and strati-graphic information from the sediment cores, $03VL\_101$ (Fig. 4.11), GS20-229-GC20 (Fig. 4.12) and GS20-229-GC21 (Fig. 4.13), that are correlated with the seismic profiles from TOPAS Line GS20-229-06 (UoB) (Fig 4.2) for the shallow part and Sparker Line $H03VL\_11022$ (Fu-gro) (Fig. 4.6) for the deeper parts of the stratigraphy. This information was combined in a Bayesian deposition model using OxCal 4.4 (Fig. 4.20 and Tables 4.2 and 4.3).
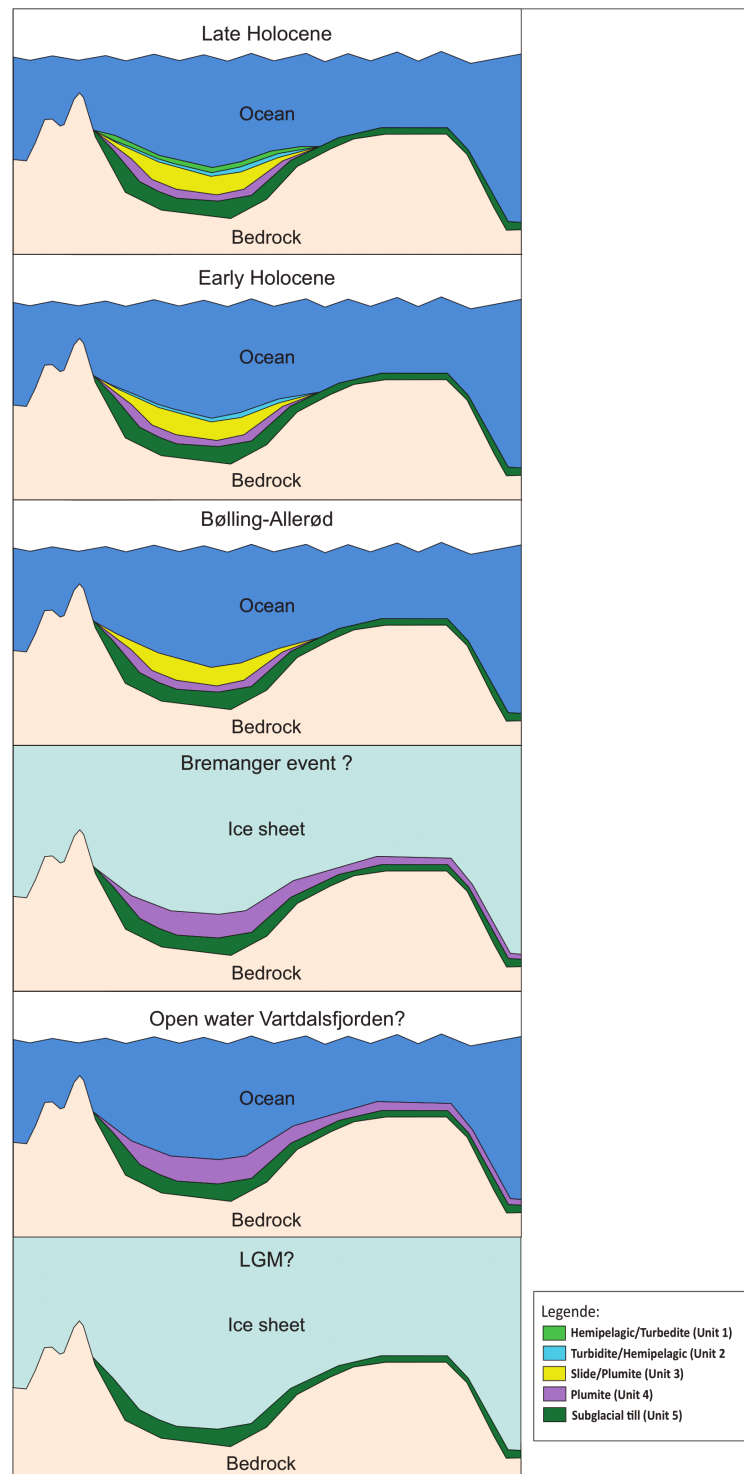
Figure 5.1: A proposed simplified deglaciation history for Vartdalsfjorden. The moraine, plumite and RB have not been dated and this is a proposed deglaciation history.

During the Last Glacial Maximum (LGM) the Fennoscandic ice sheet (FIS) covered Norway, Sweden and Finland, flowing through the fjord areas towards the edge of the continental shelf (Ottesen et al., 2016). The lowermost sedimentary unit in Vartdalsfjorden, Unit 5, is interpreted as a subglacial till. While the lack of dating precludes assigning a depositional age to Unit 5, it is plastered directly on the bedrock. This, and the fact that the ice sheet did not advance to Vartdalsfjorden during Younger Dryas (YD) (Mangerud et al., 2016), suggest that the unit was probably deposited during LGM. According to Nygård et al. (2004) (Figs. 2.4 and 5.2) the ice covered the Måløy plateau until about 18.25 cal. ka BP.

Seismic Unit 4 have been interpreted as a plumite deposit, which was possibly deposited in an ice free period after LGM. From the seismic interpretation, Unit 3 have been interpreted as plumite deposits based on the pattern of high- to low-amplitude reflectors. Unit 4 and unit 3 are separated by reflector RB. From the seismic profiles (Figs. 4.6 and 4.7) it can be observed that Unit 4 looks quite different from Unit 3 which also have some plumite deposits (Facies IIb, Table 4.1). Comparing Unit 3 and Unit 4 which both has been interpreted as plumite deposits. Unit 3 have continuous reflectors while Unit 4 has semi-continuous reflectors and small faults. This indicates that Unit 4 has been tectonised or otherwise deformed. Fig. 2.4 illustrate open water at the Måløy Plateau after the LGM (Nygård et al., 2004) which conceded with the observations from Vartdalsfjorden. Due to the lack of dating an accurate depositional age for this unit has not been determined.

Reflector RB from the Fugro data set is interpreted as an erosive contact which was likely formed during an ice advance following an early deglaciation after the LGM. This event is tentatively correlated with the Bremanger Event (Nygård et al., 2004). The reason why it correlates with the Bremanger Event are as follows: 1) the ice did not advance out as far during Younger Dryas and the dating (Tables 4.2 and 4.3) from overlaying layers indicating an older age than Bølling-Allerød. This also fits with Unit 5 being deposited during LGM and Unit 4 being deposited during a warmer period when it was open water on the Måløy Plateau (Fig. 2.4). The ice advanced at 17 cal. ka BP and retreated around 16.8 cal. ka BP during the Bremanger Event. The Bremanger Event had a regional extent, and it has therefore been suggested that it is not only a result of ice dynamics alone but might also be linked to climatic conditions (Nygård et al., 2004). Nygård et al. (2004) suggested that the Bremanger Event was the FIS responding to the cooling of the northeast Atlantic associated with Heinrich Event 1. During the Bremanger Event the ice sheet advanced in an east/northeast direction (Nygård et al., 2004). Due to the ice only being stationary for a brief period of time during the Bremanger Event no moraine or till was deposited.
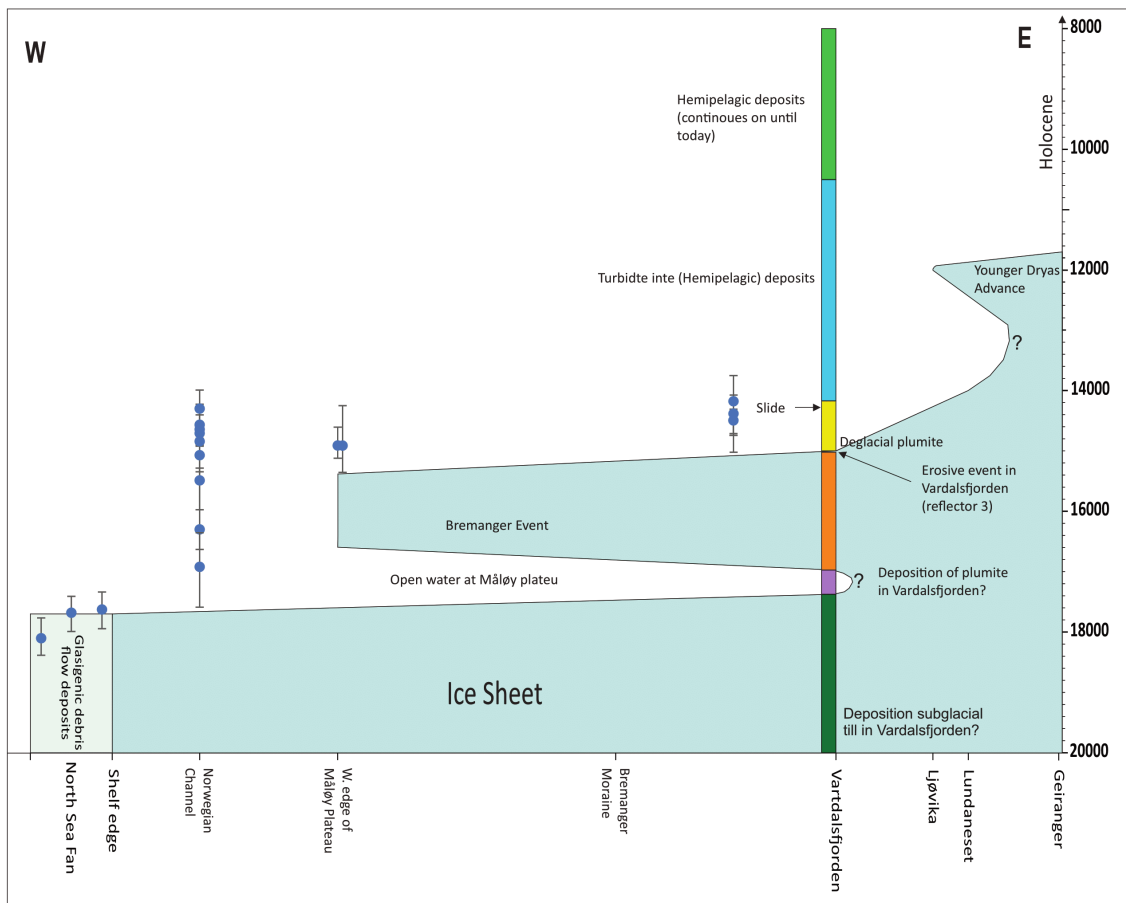
Figure 5.2: A time-distance diagram for the deglaciation of Vartdalsfjorden with proposed glacial history. Modified from Nygård et al. (2004). Datings compiled from Nygård et al. (2004) is recalibrated using Normarine18 radiocarbon calibration curve Brendryen et al. (2020), and dating for Vartdalsfjorden are acquired from tables 4.2 and 4.3 for Vartdalsfjorden.

Unit 3 (Figs. 4.20 and 4.2) indicates an age between 14,8 ka BP and 14,4 ka BP which coincides with Bølling Interstadial (also called Greenland Interstadial 1). Bølling is characterised as a warm period and is defined from 15.7 - 14.3 cal ka. BP (Mangerud et al., 1979). In this period, the ice retreated from the Bremanger moraine (Nygård et al., 2004). This unit (Figs. 4.2, 4.5, 4.6 and 4.7) is composed of of three facies: slide in the bottom (facies IIa, Table 4.1), then a plumite unit (facies IIb, Table 4.1) and several slide or slump events (facies IIa, Table 4.1) which correlates with the ice retreating, and shift in isostatic pressure creating slide events and the deposition of plumites proximal to the ice sheet. Based on the age model from Vartdalsfjorden it is likely that the deglaciation of Vartdalsfjorden happened shortly after the deglaciation of the Måløy Plateau (Fig. 5.2).

Unit 2 (Figs. 5.1 and 4.2) is turbidite deposits with some hemipelagic deposits. According to the age model Unit 2 was deposited between 10 and 6 ka BP (Fig. 4.20). Unit 1 (Figs. 5.1 and 4.2) consists of hemipelagic sediments interrupted by two turbidites. The datings (Tables 4.2 and 4.3) indicate that the unit was deposited during mid- to late-Holocene. Holocene lasted from 11.6 ka until today (Björck et al., 1998). In summary, Unit 3 was the start of the deglaciation sediment deposited in Vartdalsfjorden. As the climate gradually warmed up, and isotatic and eustatic processes occurred the sediments progressed from plumite and slides to turbidite sequences. Lastly, hemipelagic sediments were deposited.

5.2 Pockmarks and fluid flow

5.2.1 Pockmark distribution

The pockmarks in Vartdalsfjorden create a pattern for their localisation in the fjord. They are all located in the middle of the fjord basin (Figs. 4.1 and 4.2). The structures are all located in hemipelagic sediments with slide deposits underneath. However, the slides are located much further down in the sediment and has most likely not influenced the distribution of the pockmarks.

The seismic profiles acquired from Vartdalsfjorden only passes through a few of the identified pockmarks. The pockmarks observed are all located within Unit 1 which has been interpreted as hemipelgaic sediments with two turbidites, deposited during the Holocene. Based on the seismostratigraphy Unit 1 is approximately 7 m thick. The thickness of the Holocene sediments and the underlying topography govern the distribution and size of the pockmarks found in temperate eustrine conditions (Brothers et al., 2012). The pockmarks in Vartdalsfjorden are located in the centre where the Holocene sediments are thickest and undisturbed.

Hovland et al. (2002) found that the density of pockmarks varies as a consequence of fluid flow, underlying geology and the type of seabed sediments. In Vartdalsfjorden all the pockmarks occurs in a wide line which might indicate a weakness zone since pockmarks might be a significant indicator for subsurface hydraulic activity (Hovland et al., 2002). The reason why we might only observe the pockmarks in this location is if the gas seeps through permeable sand layers in the turbidite deposits. The turbidite deposits are mainly located in the centre of the fjord (Figs. 4.5 and 4.6). From Fig. 4.9 bright spots can be observed, and a chimney structure (Fig. 4.8) is observed deeper in the stratigraphy. The chimney structure indicates fluid flow or gas seep deeper in the stratigraphy and the gas enhanced reflectors below the pockmarks indicate gas seepage.

5.2.2   Pockmark morphology

The pockmarks in Vartdalsfjorden can be compared to other observed pockmarks based on their morphological characteristics (Table 5.1), such as the pockmarks in Oslofjorden (Webb et al., 2009) and Belfast Bay, Maine (Rogers et al., 2006). Webb et al. (2009) found no correlation between sediment thickness and type of sediment. However, Rogers et al. (2006) found a link between the Holocene mud deposits observed in the Belfast Bay and the size of the pockmarks. The largest pockmarks where found in the area with the thickest Holocene mud. This association between the Holocene mud and the size of the pockmarks indicates strongly that the mud contributes with gas to the sediment column (Rogers et al., 2006). In Vartdalsfjorden, the pockmarks are located at a similar depth and it is therefore not possible to comment on this correlation between the sediment thickness and the size of the pockmarks. The Holocene hemipelagic sediments have a low permeability and thus the fluid is likely to seep through localised failures and/or permeable strata like the turbidite deposits.

Based on the size and shape of the pockmarks in Vartdalsfjorden, they can be categorised as *"normal" pockmarks* according to Hovland et al. (2002). A *"normal" pockmark* is defined as a pockmark that measures between 10-700 m in diameter and from 1-45 m deep (Hovland et al., 2002). The angle of slope for the pockmarks is between 3-7 %. This low angle of slope will not affect the sedimentation rates such as an upwelling hypothesis presented by Webb et al. (2009). Active seepage, both periodic and constant, would work against sediment accumulation and keep the pockmark structure relatively free of new sediments (Hovland et al., 2002). How long the pockmark structures are preserved depends on the sedimentation rate in the area. If the sedimentation rate was zero or low, the pockmarks would be preserved for a longer time period. However, in an area such as Vartdalsfjorden, were the sedimentation rate is high due to both river deposits and material transported in through the fjord causes the structures to gradually fill up of sediments if the structures are not active.

Table 5.1: Overview of other documented pockmark fields with similar morphology as the pockmarks in Vartdalsfjorden. References: (1) This study. (2) Webb et al. (2009). (3) Audsley et al. (2019). (4) Rogers et al. (2006). (5) Roy et al. (2014). (6) Roy et al. (2015). (7) Roy et al. (2016). (8) Roy et al. (2019). (9) Pau et al. (2014).

Region	Width	Depth	Geometric shape	Reference
Vartdalsfjorden	32-81	0.8-1.4	Circular	1
Inner Oslofjorden	16-100	1-12	Circular to elliptical	2
Western Scotland	16-100	1-12	Elongated and circular	3
Belfast Bay	Up to nearly 300	20 - 30	Circular	4
Inner Isfjorden	18-213	1-7	Circular to elongated	5
Billefjorden	15-97	1-4	Circular, some elongated	6
Adventfjorden	35-114	1-6	Circular, some elongated	6
Tempelfjorden	15-102	1-3	Circular	6
Grønfjorden	10-265	1-10	Circular, some elongated	6; 7
Nordfjorden	7-260	1-8	Circular, some elongated	6; 8
(SW Barent Sea)	20-25	1.5-2	Mostly circular	9

5.2.3 Formation age for the pockmarks in Vartdalsfjorden

One of the objectives for this study was to determine the formation age of the pockmarks. To determine the age of the pockmarks, the lowermost reflector underneath the pockmark that is bending down is traced into the dated core stratigraphy. This reflector corresponds to reflector 1.2 (Figs. 4.5, 4.2, 4.3 and 4.4). This is the first reflector that bends down showing evidence of the pockmark. This therefore gives a minimum age for the formation of the pockmark. Reflector 1.2 is dated to a minimum age of 3.8 ka cal BP. The uppermost straight reflector underneath the pockmarks (black line, Fig. 5.3) indicate the maximum age. The depth of this reflector gives the maximum age of 6.6 ka cal BP for the pockmark formation. The uppermost reflector underneath the pockmark that is straight can be traced at the same depth for the 5 pockmarks, on the seismic lines (Figs. 4.2 and 4.5).
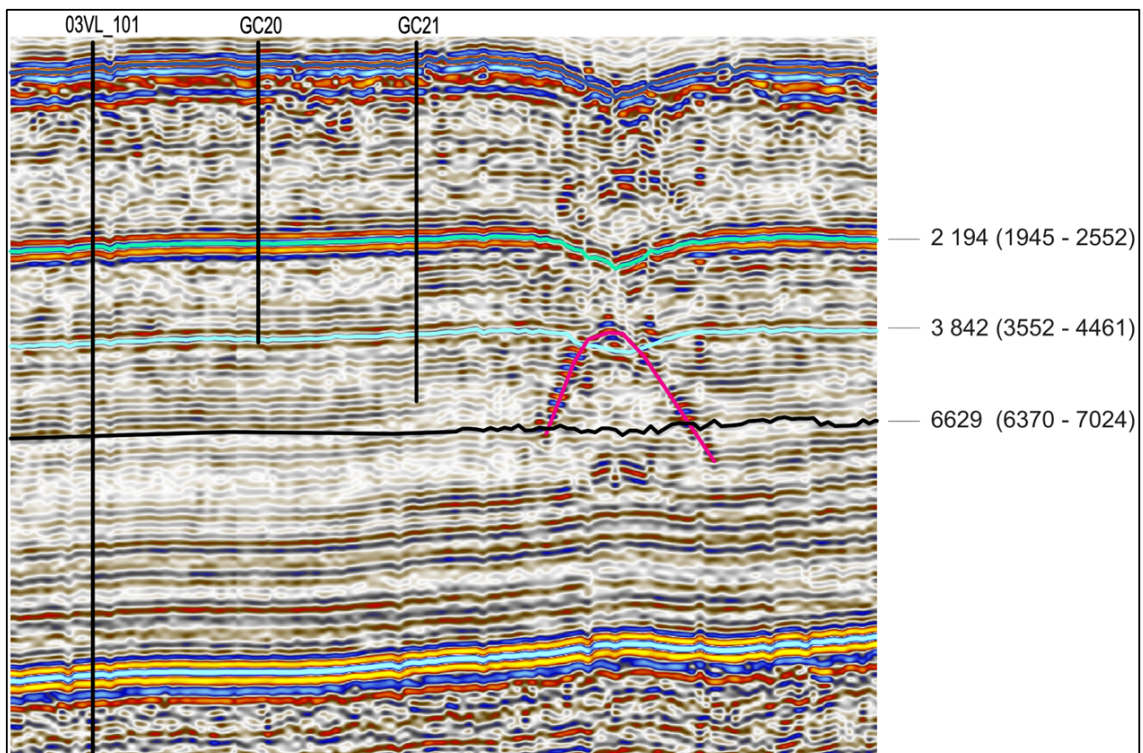
Figure 5.3: The formation age for the pockmarks in Vartdalsfjorden. The green reflector corresponding to an age of 2.2 ka BP is reflector R1.1, and the light blue corresponding to the age of 3.8 ka BP is reflector 1.2. Both reflector R1.1 and R1.2 is shown in Figs. 4.5 and 4.2.

5.2.4 Fluid flow

The origin of gas that migrate through the sediments can be bacterial action or seepage from deeper reservoirs (Gylland and Vries, 2008). Bacterial action or biological activity is defined as sub-bottom or bottom-dwelling organisms (Hovland and Judd, 1988). This gas has been observed to migrate through the seabed in free form (Gylland and Vries, 2008). Migration of gas is a complex balance of several processes and it is difficult to establish a general theory which describes the processes at hand. This is due to the fact that the observations can only be made from the surface and thus making it difficult to clarify if the hypothesis is consistent with reality (Gylland et al., 2007).

Natural gases can occur in two forms, either in free or dissolved form (Gylland et al., 2007). Hovland and Judd (1988) uncovered that the gas found in shallow marine sediments consists both of gas formed from bacterial action within the sediments and gas that has migrated from deeper reservoirs. Two types of migration of free gas can occur a slow-rate type or a blow-out type (Gylland et al., 2007). According to Hovland et al. (2002) it has been suspected that the fluids escaping through the sediments migrate very slowly to the surface. For this study the slow-rate type is the most relevant.
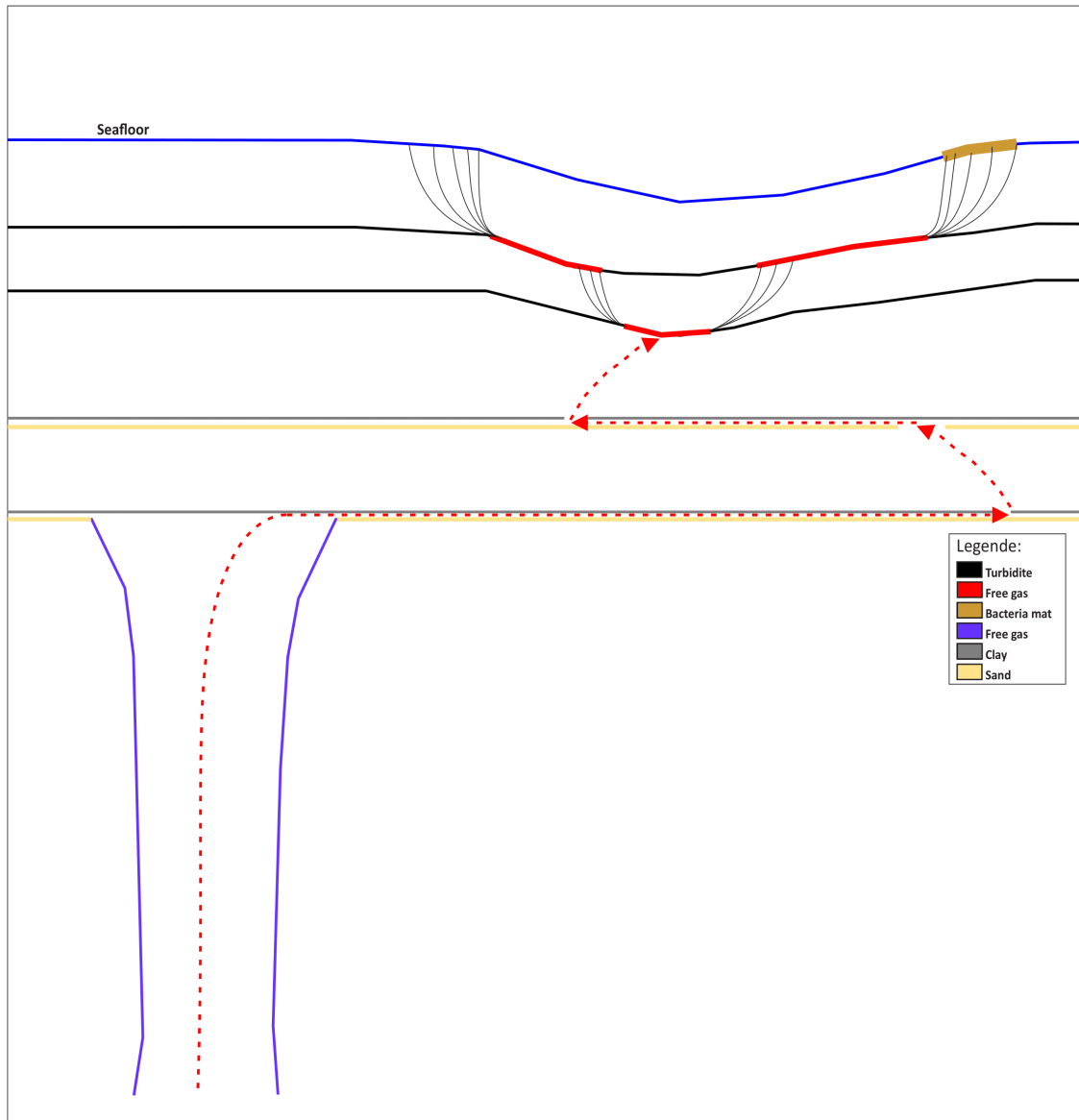
Figure 5.4: A proposed fluid flow model for the pockmarks in Vartdalsfjorden.It is proposed that the fluid or gas originates from the area with the chimney and follows the permeable layers in the turbidite to weakness zones in the impermeable clay layer in the turbidites.

To create pockmarks, four fluids supplies have been recognised and generally considered as potential source; thermogenic fluid (principally gas), biogenic, volcanic or hydrothermal gas or ground water (Hovland and Judd, 1988). Three of these are relevant for this study, thermogenic fluid, biogenic and ground water.

In the deeper part of the stratigraphy a chimney structure can be observed (Figs. 4.8 and 4.10). Gas from deeper sediments might seep up through the chimney and then follow the turbidite deposits (permeable layers) (Fig. 5.4). The chimney is corroboration that fluid flow occurred in Vartdalsfjorden possibly before the formation of the pockmarks. In core $03VL\_101$, some closely spaced thin laminae of black clay (possible organic) with fine to medium gravel-sized pockets of black matter (possible organic) in the unit between 13.82-27.00 m, indicate that there might be organic sediments in the stratigraphy, and is a potential source for the gas.

The gas might follow the permeable sandy layers in the turbidite deposits that are overlain by an impermeable clay layer trapping the gas in the sand layer. The gas follows the turbidite deposits and seep upwards in a localised failures or permeable strata in the clay. From Fig. 5.4 gas-enhanced reflectors can be observed, but not directly underneath the pockmark. This might be due to the gas directly underneath the pockmark seeping out. The lack of gas directly underneath the pockmarks and gas enhanced reflectors have also been observed by other (Rogers et al., 2006).

5.3   Formation of pockmarks

There is a limited amount of studies of pockmarks in Norwegian fjords that have been conducted which makes these pockmarks in Vartdalsfjorden interesting. Commonly, pockmarks occur in soft, fine-grained sediments (Rise et al., 1999), and from the core stratigraphy (Figs. 4.12 and 4.13) it can be observed that the sediments are quite fine grained with the exception of the two turbidite deposits. The most recognised theory for pockmark formation is through gas or fluids escaping the sediments (King and MacLean, 1970). However, several other formation mechanisms such as actions from above the seabed, biological activity and mechanisms related to the last ice age have also been proposed. From above the seabed entails factors such as iceberg drop-stones, and man-made artefacts such as wrecks and bombs. The biological activity occurs in the form of sub-bottom or bottom-dwelling organisms (Hovland and Judd, 1988).

The results from the core stratigraphic, microbial taxonomy and pore fluid analyses have no evidence for the presence of gas or fluids within the sediments. However, bright spots observed in the acoustic data suggest that there are accumulations of free gas underneath

the pockmarks (Fig. 4.9) (Rogers et al., 2006). This indicate that the pockmarks may not continuously release gas. The gas might instead be released periodically or during certain events. GS20-229-GC21 was taken in the centre of the pockmarks and from Fig. 4.9 the gas enhanced reflectors can be observed on the walls of the pockmarks. Therefore, the evidence of gas or fluids escaping might not have been collected by the core.

However, for the formation mechanisms of pockmarks in Vartdalsfjorden three hypothesis have been presented which includes; a) release of ground water from bottom sediments, or from bedrock structures, b) compaction of soft sediments at the fjord bottom followed by seepage of pore water and/or trapped gas related to slide events, and c) release of shallow gas, either periodical or during an event.

5.3.1   Release of ground water from bottom sediments, or from bedrock structures

Release of ground water from bottom sediments, or from bedrock structures has been a proposed formation mechanism for the pockmarks in Ullsfjorden in Troms, Northern Norway (Plassen and Vorren, 2003) and in inner Oslofjorden (Hammer and Webb, 2010). In Ullsfjorden it has been suggested that the ground water seepage followed the tectonic ligaments (Plassen and Vorren, 2003). In Vartdalsfjorden no tectonic ligaments can be observed. The release of ground water from bottom sediments is not very possible hypothesis due to no faults or other structures being observed in the study area. In addition, the geochemical and geobiological research have no indication of fresh water in the sediments. Therefore, it can be concluded that flow of ground water from bottom sediments, or from bedrock structures are not the likely formation mechanisms for the formation of the pockmarks observed.

5.3.2   Compaction of soft sediments at the fjord bottom followed by seepage of pore water and/or trapped gas related to slide events

Harrington (1985) suggested that a dewatering process could lead to the formation of an acoustic voids in one situation and pockmarks in another. Several factors could influence whether an acoustic voids or pockmarks were created such as time of formation, grain size, water depth, and particularly porosity difference between layers and overburden. A theory was proposed that the acoustic voids was formed in relatively shallow water, not long after the last ice had retreated before the sea level transgression (Harrington, 1985). In Vartdalsfjorden several landslides can be observed, as well as a dewatering processing.

This formation mechanisms has also been suggested for the pockmarks in inner Oslofjorden

(Webb et al., 2009). Before the pore pressure in the sediments sinks to zero through consolidation, the shear strength is related to water content, effective stress, and the structure of the sediments. Normally, the water content will be reduced gradually as the effective stress increases with time as a result of consolidation and dehydrating of the sediments (Wang et al., 2015).

In the bottom of the core shear strength will be higher than at the top due to overlying sediments or as a result of dehydration. This can be explained by masses, such as slides, that have consolidated the sediment and created over-pressure so that the pore water seeps out of the sediment. Or it might be pore water might be trapped in a sandy layer inside or underneath a permeable layer of clay and over-pressure occurs in the sediments. There are several consequences to over-pressure, with burial of the sediments will the stress will increase and the pore fluids will carry a lot of the weight from the overlaying sediments.This will result in a reduced contact between the sediment grains. The sediments with a high fluid content will not be compressed and will therefore remain unconsolidated. The increase in shear strength will also be reduced, the density will remain low and if the fluids consists of water it can cause an local increase in temperature which will result in increased energy. The increased energy and pressure in the sediments to might cause the fluids and sediments to seep upwards (Judd and Hovland, 2009).

In Vartdalsfjorden several submarine slides can be observed in Unit 3. However, the pockmarks does not penetrate far enough in the sediment column that they penetrate into the submarine slide sediments. In addition, the dating indicate that the top of the big slides in Vartdalsfjorden have a minimum age of about 14.3 ka BP, and the pockmarks have a minimum formation age of 3.8 ka BP and a maximum age of 6.6 ka BP. Based on these findings the formations mechanisms for the pockmarks in Vartdalsfjorden are not related to the compaction of soft sediments at the fjord bottom followed by seepage of pore water and/or trapped gas related to slide events.

5.3.3   Release of shallow gas, either periodical or during an event

In Vartdalsfjorden shallow gas might be the most likely formation mechanism due to a bacterial mat being observed on the edge of one of the pockmarks (Fig. 5.5). An bacterial mat need nutrients to grown and it would most likely not be observed if it was fresh water seepage from the pockmark. In addition, a chimney structure and bright spots was observed on the seismic (Figs. 4.8, 4.10 and 4.9).

On the Fugro data set on line 6 (Fig. 4.10) a chimney is observed. The chimney is vertical to sub-vertical anomaly with circular or elliptical platforms and generally seismic amplitude
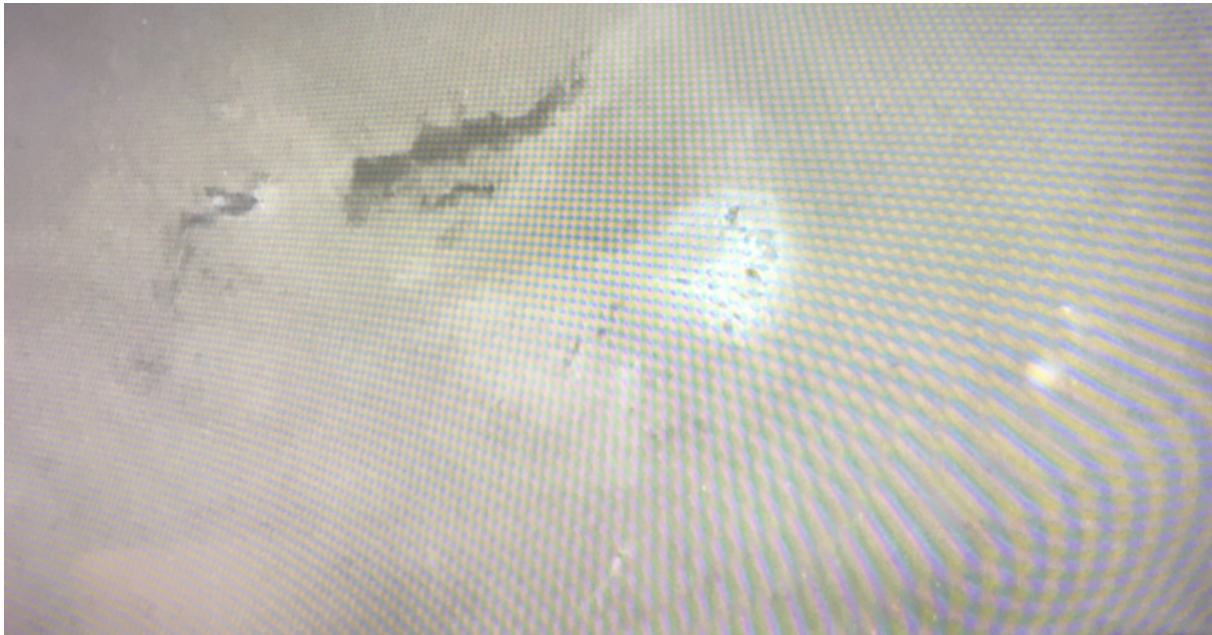
Figure 5.5: The bacterial mat observed in Vartdalsfjorden inside a pockmark. Due to upgrades at the department, getting a picture with better quality was not possible. This picture was taken with a cell phone of the computer screen during the summer cruise of 2020 by Haflidi Haflidason.

blanking and discontinuous/chaotic reflectors can be observed. If fluids were to migrate from a sub-surface reservoir of CO_2/CH_4 and reach the base of the chimneys, then the chimneys could act as a pathway for the gas and fluids. Acting as a pathway for the fluids, by allowing upward migration towards the seafloor, and into the water column (Callow et al., 2021).

Methane can be formed in shallow sediments by microbial activity. If methagonesis results in the elevation of methane concentration beyond the solubility limit any excess production will lead to the formation of methane gas bubbles. The bubbles are buoyant and if the conditions persist they will rise towards the surface until the bubbles reach a zone of undersaturated pore water. Here they will be re-dissolved. Normally the methane bubbles will not escape to the seabed for this reason (Judd and Hovland, 2009).

From the geochemical and geobiological data there where no evidence of methane, which indicates that either the pockmarks are not active any more or they are only active in certain periods or during events. A tidal variation of gas fluxes have been observed and is consistent with gas transport through fractures that open at low tide in response to reductions in confining pressure of changes of gas solubility (Callow et al., 2021). To determine whether they are active or inactive further research is needed. One way to do this would be to create a similar measuring grid and/or CTD stations as Henriksen and Dale (2018) in Vartdalsfjorden around the pockmarks . Henriksen and Dale (2018) created a rectangular grid with 16 observation points in the Stampa Bay in Aurlandsfjorden. This setup measured the water depth,

temperature, density, salinity, oxygen, chlorophyll, and turbidity. By placing the measure apparatus in the centre of the pockmarks the potential seepage can be measured.

5.4   Biogeochemical processes

Pore water composition is a good indicator for ongoing biogeochemical processes and is generally controlled by the amount and availability of organic carbon. This in turn act as a strong regulator of microbial activity which ultimately determines the pore water composition. The geochemical composition of the fluids investigated here reveals that the sediments are suboxic to anoxic already in the top layer with both O_2 and NO_3^- below the detection limit at 1 cm and 5 cm, respectively. Based on our results it is evident that the organic load must be relatively high as the microbes depletes the oxygen during mineralization of organic carbon already at very shallow depth. A high microbial activity is also indicated by the high and increasing concentrations of ammonium (Figs. 4.14 and 4.15), caused by the high mineralization rates releasing ammonium into the pore fluids.

Below the shallow oxic zone and above the deeper sediments, the suboxic zone is located. In the suboxic zone the processes of denitrification and manganese and iron reduction occur (Burdige, 2006). In Figs. 4.14 and 4.15 a clear signal of manganese and iron reduction can be identified in the upper part of the core. However, as nitrate measurements were below the detection limited the location of denitrification can not be specifically pinpointed but it is assumed to be located in a shallow zone right below the oxygen depletion zone.

Manganese and iron are stable under the oxygenated conditions encountered in the water column, but both quickly becomes unstable after the burial below the oxic layers of the sediments (Konhauser, 2007). In GC20 and GC21 the concentration of manganese is quite similar. Both decrease downwards, before slightly increasing at the bottom. Iron (Fe) reduction generally occurs higher up in the core than manganese (Mn) reduction (Burdige, 2006), this general pattern is also observed in the pore water samples from Vartdalsfjorden.

Below the suboxic zone the zone are referred to as anoxic, and here sulphate reduction and methanogenesis occur (Burdige, 2006). Throughout both cores there is a clear signal of strong sulphate reduction as seen by the depletion of sulphate in the pore fluids. While methane was not measured there is nothing in the microbial data which indicates that methanogens plays any major role, as inferred from the lack of typical methanogenic organisms such as members of methanococcales, methanomicrobiales and methanosarcinales . In addition, we see no evidence of a large population of methanotrophs which might have been present at the very top layers if methane had been diffusing out of the sediments. In GC20 and GC21 the concentrations of SO_4^{2-} are comparable but from around 1 m to the bottom of the core

GC21, the concentration is slightly higher. This can indicate that the concentration of organic material is slightly higher here and/or that the decomposition of organic material is slightly higher inside the pockmark than outside.
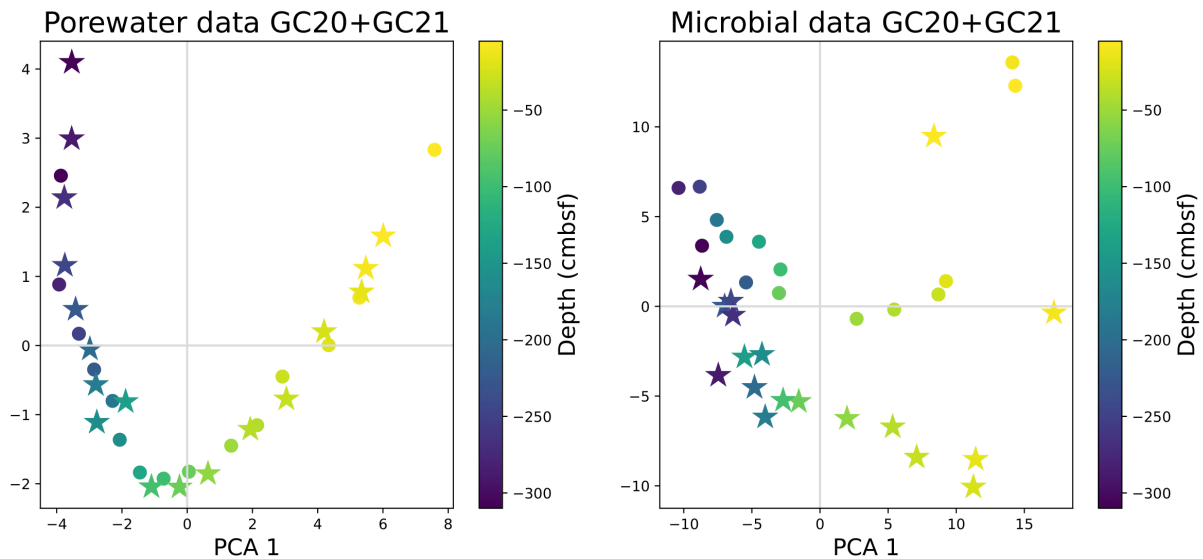
Figure 5.6: PCA plot for both GC20 and GC21 for pore water and microbial data. The dots represent GC20 and the stars GC21.

When comparing the variability of the pore fluid in the pore fluid in the two cores ((Fig. 5.6).) it becomes evident that the fluids in the two cores are very similar. This suggest that there are no active fluid flow in the pockmarks. The same is true when comparing the variability in the microbial communities although slight differences between the two sites are observed in the top layers. Hence, neither the pore fluid data nor the microbial (Fig. 5.6) suggest that there is any methane or fresh water present in the pockmarks when the cores where acquired. However, from the seismic data set several bright spots can be observed indicating that there is gas present (Fig. 4.9). The reason for this might be that the that the gas has a different path up through the sediments than where the cores were taken (Fig 5.4).

6. Summary and conclusions

The main objective of this study is to determine whether the pockmarks in Vartdalsfjorden are active or inactive today. To determine this the formation of the pockmarks, age and their biogeochemical character have been studied. The main concluding results are;

The sedimentary history of Vartdalsfjorden can be summarised as follows; The lower units (Unit 5, Unit 4 and the reflector RB) age is not determined but based on the seismostratigraphy it has been concluded that; Unit 5 was deposited during LGM due to it being located directly on the bedrock. Then the ice retreated and it was open water into Vartdalsfjorden. RB is an erosive contact and was probably formed when the ice advanced during the Bremanger event. Then the ice retreated and Unit 3 was deposited during Bølling-Allerød. Unit 2 is turbidite deposited interbedded with some hemipelgaic deposits, this unit was deposited during the Early Holocene. Last Unit 1 deposited from mid- to late-Holocene until today. Unit 1 consists of hemipelagic sediments with two turbidite sequences.

Based on the seismic, core stratigraphy, geochemical and geobiological processes we can conclude with the following regarding the pockmarks:

- The bathymetri shows that in Vartdalsfjorden at least 19 pockmarks occur at a water depth of approximately 360 m. The pockmarks are symmetric and circular, with an average with of 45 m and 1 m deep. They are classified as *"normal" pockmarks*.

- Based on the age model of the Vartdalsfjorden sedimentary deposits ^{14}C the pockmarks formation age and the big slides observed on the seismic is not related. The formation age of the pockmarks have a minimum age of 3.8 cal ka BP and a maximum age of 6.6 cal ka BP, while the big slide deposit observed under the pockmarks transpired about 14.3 cal ka BP.

- The pore water analysis and microbial taxonomy shows no evidence for the seepage of gas or fresh water. There is no significant difference between the two cores, one taken outside the pockmark and one inside. Based on these findings it is not easy to determine whether the pockmarks are active today or what keeps them open. However, from the seismic bright spots which indicate gas.

- Based on the observation and analysis the most likely hypothesis for the formation is release of shallow gas, either periodical or during an event.

7. Further work

Several questions remain unanswered and further work is needed to fully understand the pockmark formation mechanisms and whether or not it is methane seepage. Getting a better understanding of why the pockmarks are not filled in by sediments is important, and more surveillance is needed to achieve this.

By placing a measuring device in the centre of the pockmarks it would be possible to measure variations over a longer time period and put it into context with yearly variations. It would be interesting to create a measuring grid and/or CTD stations similar to what Henriksen and Dale (2018) created in Aurlandsfjorden. By creating a similar setup and measuring the water depth, salinity, temperature, density, oxygen, chlorophyll and turbidity a better understanding of the pockmarks formation might be achieved.

In Vartdalsfjorden only 5 of 19 pockmarks were transected by seismic lines. It would therefore be interesting to get seismic data through all the pockmarks and take more gravity cores within the remaining pockmarks. In addition, the gravity cores should not only be taken in the centre of the pockmarks but also in the pockmarks walls since the bright spot observed on the seismic where not in the centre of the pockmark. It would also be interesting to do more geomicrobial and geochemical analysis of the microbial communities in the sediments.

A bacteria mat was observed in one of the pockmarks. Studying the microbial community might reveal the source of the gas or fluid escaping the sediment. Therefore, it would be advantageous to get a sample of the bacteria mat and perform PCR and DNA analysis.

In, addition it would be advantageous to get acquire a core deeper into the sediments to possibly determine if finding there are organic material deeper in the stratigraphy which can reveal about the source of the gas.It would also be preferable to analyse the black laminae and black gravel size pockets of black matter observed in core $03VL_101$ to figure out whether or not it is organic, and if it is organic which kind of microbial communities are present in the black matter.

References

Aarseth, I. (1997). Western Norwegian fjord sediments: age, volume, stratigraphy, and role as temporary depository during glacial cycles. *Marine Geology 143*(1-4), 39–53.

Aarseth, I., Ø. Lønne, and O. Giskeødegaard (1989). Submarine slides in glaciomarine sediments in some western Norwegian fjords. *Marine Geology 88*(1-2), 1–21.

Aksnes, D. L., J. Aure, P.-O. Johansen, G. H. Johnsen, and A. G. V. Salvanes (2019). Multidecadal warming of Atlantic water and associated decline of dissolved oxygen in a deep fjord. *Estuarine, Coastal and Shelf Science 228*, 106392.

Audsley, A., T. Bradwell, J. Howe, and J. Baxter (2021). Spatial Relationships between Pockmarks and Sub-Seabed Gas in Fjordic Settings: Evidence from Loch Linnhe, West Scotland. *Geosciences 11*(7), 283.

Audsley, A., T. Bradwell, J. A. Howe, and J. M. Baxter (2019). Distribution and classification of pockmarks on the seabed around western Scotland. *Journal of Maps 15*(2), 807–817.

Björck, S., M. J. Walker, L. C. Cwynar, S. Johnsen, K.-L. Knudsen, J. J. Lowe, and B. Wohlfarth (1998). An event stratigraphy for the Last Termination in the North Atlantic region based on the Greenland ice-core record: a proposal by the INTIMATE group. *Journal of Quaternary Science: Published for the Quaternary Research Association 13*(4), 283–292.

Brendryen, J., H. Haflidason, Y. Yokoyama, K. A. Haaga, and B. Hannisdal (2020). Eurasian Ice Sheet collapse was a major source of Meltwater Pulse 1A 14,600 years ago. *Nature Geoscience 13*(5), 363–368.

Brothers, L. L., J. T. Kelley, D. F. Belknap, W. A. Barnhardt, B. D. Andrews, C. Legere, and J. E. H. Clarke (2012). Shallow stratigraphic control on pockmark distribution in north temperate estuaries. *Marine Geology 329*, 34–45.

Burdige, D. J. (2006). *Geochemistry of marine sediments*. Princeton University Press.

Callow, B., J. M. Bull, G. Provenzano, C. Böttner, H. Birinci, A. H. Robinson, T. J. Henstock, T. A. Minshull, G. Bayrakci, A. Lichtschlag, et al. (2021). Seismic chimney characterisation in the North Sea–Implications for pockmark formation and shallow gas migration. *Marine and Petroleum Geology 133*, 105301.

Clark, P. U., A. S. Dyke, J. D. Shakun, A. E. Carlson, J. Clark, B. Wohlfarth, J. X. Mitrovica, S. W. Hostetler, and A. M. McCabe (2009). The last glacial maximum. *science 325*(5941), 710–714.

Dean, W. E. (1974). Determination of carbonate and organic matter in calcareous sediments and sedimentary rocks by loss on ignition; comparison with other methods. *Journal of Sedimentary Research 44*(1), 242–248.

Emmanouilidis, A., G. Messaris, E. Ntzanis, P. Zampakis, I. Prevedouros, D. A. Bassukas, and P. Avramidis (2020). CT scanning, X-ray fluorescence: Non-destructive techniques for the identification of sedimentary facies and structures. *Revue de micropaléontologie 67*, 100410.

Forwick, M., N. J. Baeten, and T. O. Vorren (2009). Pockmarks in Spitsbergen fjords. *Norwegian Journal of Geology/Norsk Geologisk Forening 89*.

Froelich, P., G. Klinkhammer, M. L. Bender, N. Luedtke, G. R. Heath, D. Cullen, P. Dauphin, D. Hammond, B. Hartman, and V. Maynard (1979). Early oxidation of organic matter in pelagic sediments of the eastern equatorial Atlantic: suboxic diagenesis. *Geochimica et cosmochimica acta 43*(7), 1075–1090.

Fugro (2018). Measured and Derived Geotechnical Parameters and Final Results, Fjord Crossing E39 - Marine Ground (50013-Ra(02)) Investigations.

Google (2022). Map of Norway.

Gylland, A. and M. Vries (2008). The effect of a gas blow-out on shallow offshore foundations exposed to static loads.

Gylland, A. S., E. Kristiansen, and M. Vries (2007). Gas flow effects on the stability of shallow offshore foundations. In *Proceedings of the 18th European Young Geotechnical Engineers Conference, Ancona, Italy*, pp. 17–20.

Hammer, Ø. and K. E. Webb (2010). Piston coring of Inner Oslofjord pockmarks, Norway: constraints on age and mechanism. *Norwegian Journal of Geology/Norsk Geologisk Forening 90*.

Hansbo, S. (1957). *New approach to the determination of the shear strength of clay by the fall-cone test*.

Hansen, K. E., J. Giraudeau, A. Limoges, G. Massé, A. Rudra, L. Wacker, H. Sanei, C. Pearce, and M.-S. Seidenkrantz (2022). Characterization of organic matter in marine sediments to estimate age offset of bulk radiocarbon dating. *Quaternary Geochronology 67*, 101242.

Harrington, P. (1985). Formation of pockmarks by pore-water escape. *Geo-Marine Letters 5*(3), 193–197.

Heiri, O., A. F. Lotter, and G. Lemcke (2001). Loss on ignition as a method for estimating organic and carbonate content in sediments: reproducibility and comparability of results. *Journal of paleolimnology 25*(1), 101–110.

Henriksen, H. and T. Dale (2018). Groundwater discharge from a rock-slope failure system in phyllitic rocks influencing fjord basin hydrodynamics, Stampa in Aurland, western Norway.

Hjelstuen, B. O., H. Haflidason, H. P. Sejrup, and A. Lyså (2009). Sedimentary processes and depositional environments in glaciated fjord systems—evidence from Nordfjord, Norway. *Marine Geology 258*(1-4), 88–99.

Hovland, M., J. V. Gardner, and A. Judd (2002). The significance of pockmarks to understanding fluid flow processes and geohazards. *Geofluids 2*(2), 127–136.

Hovland, M. and A. Judd (1988). *Seabed pockmarks and seepages: Impact on geology, biology and the marine environment.*

Hughes, A. L., R. Gyllencreutz, Ø. S. Lohne, J. Mangerud, and J. I. Svendsen (2016). The last Eurasian ice sheets–a chronological database and time-slice reconstruction, DATED-1. *Boreas 45*(1), 1–45.

Judd, A. and M. Hovland (2009). *Seabed fluid flow: the impact on geology, biology and the marine environment.* Cambridge University Press.

Kartverket (2022). Vartdalsfjorden.

Kelley, J. T., S. M. Dickson, D. F. Belknap, W. A. Barnhardt, and M. Henderson (1994). Giant sea-bed pockmarks: evidence for gas escape from Belfast Bay, Maine. *Geology 22*(1), 59–62.

King, L. H. and B. MacLean (1970). Pockmarks on the Scotian shelf. *Geological Society of America Bulletin 81*(10), 3141–3148.

Kjennbakken, H., H. P. Sejrup, and H. Haflidason (2011). Mid-to late-Holocene oxygen isotopes from Voldafjorden, western Norway. *The Holocene 21*(6), 897–909.

Konhauser, K. O. (2007). *Introduction to geomicrobiology.* John Wiley & Sons.

Lekens, W., H. P. Sejrup, H. Haflidason, G. Petersen, B. Hjelstuen, and G. Knorr (2005). Laminated sediments preceding Heinrich event 1 in the Northern North Sea and Southern Norwegian Sea: origin, processes and regional linkage. *Marine Geology 216*(1-2), 27–50.

Mangerud, J., I. Aarseth, A. L. Hughes, Ø. S. Lohne, K. Skår, E. Sønstegaard, and J. I. Svendsen (2016). A major re-growth of the Scandinavian Ice Sheet in western Norway during Allerød-Younger Dryas. *Quaternary Science Reviews 132*, 175–205.

Mangerud, J., E. Larsen, O. Longva, and E. Sønstegaard (1979). Glacial history of western Norway 15,000–10,000 bp. *Boreas 8*(2), 179–187.

NGU (2022). Berggrunnskart.

Nygård, A., H. P. Sejrup, H. Haflidason, M. Cecchi, and D. Ottesen (2004). Deglaciation history of the southwestern Fennoscandian Ice Sheet between 15 and 13 14C ka BP. *Boreas 33*(1), 1–17.

Ottesen, D., C. R. Stokes, R. Bøe, L. Rise, O. Longva, T. Thorsnes, O. Olesen, T. Bugge, A. Lepland, and O. B. Hestvik (2016). Landform assemblages and sedimentary processes along the Norwegian Channel Ice Stream. *Sedimentary Geology 338*, 115–137.

Pau, M., Ø. Hammer, and S. Chand (2014). Constraints on the dynamics of pockmarks in the SW Barents Sea: evidence from gravity coring and high-resolution, shallow seismic profiles. *Marine Geology 355*, 330–345.

Peacock, D. C. and G. J. Banks (2020). Basement highs: Definitions, characterisation and origins. *Basin Research 32*(6), 1685–1710.

Plassen, L. and T. O. Vorren (2003). Fluid flow features in fjord-fill deposits, Ullsfjorden, North Norway. *Norsk Geologisk Tidsskrift 83*(1), 37–42.

Rise, L., J. Sættem, S. Fanavoll, T. Thorsnes, D. Ottesen, and R. Bøe (1999). Sea-bed pockmarks related to fluid migration from Mesozoic bedrock strata in the Skagerrak offshore Norway. *Marine and Petroleum Geology 16*(7), 619–631.

Rogers, J. N., J. T. Kelley, D. F. Belknap, A. Gontz, and W. A. Barnhardt (2006). Shallow-water pockmark formation in temperate estuaries: a consideration of origins in the western gulf of Maine with special focus on Belfast Bay. *Marine Geology 225*(1-4), 45–62.

Rothwell, R. G. et al. (2015). Twenty years of XRF core scanning marine sediments: what do geochemical proxies tell us? In *Micro-XRF studies of sediment cores*, pp. 25–102. Springer.

Roy, S., M. Hovland, and A. Braathen (2016). Evidence of fluid seepage in Grønfjorden, Spitsbergen: implications from an integrated acoustic study of seafloor morphology, marine sediments and tectonics. *Marine Geology 380*, 67–78.

Roy, S., M. Hovland, R. Noormets, and S. Olaussen (2015). Seepage in Isfjorden and its tributary fjords, West Spitsbergen. *Marine Geology 363*, 146–159.

Roy, S., K. Senger, A. Braathen, R. Noormets, M. Hovland, and S. Olaussen (2014). Fluid migration pathways to seafloor seepage in inner Isfjorden and Adventfjorden, Svalbard. *Geological controls on fluid flow and seepage in western Svalbard fjords, Norway. An integrated marine acoustic study*.

Roy, S., K. Senger, M. Hovland, M. Römer, and A. Braathen (2019). Geological controls on shallow gas distribution and seafloor seepage in an Arctic fjord of Spitsbergen, Norway. *Marine and Petroleum Geology 107*, 237–254.

Saenko, O. A., J. C. Fyfe, and M. H. England (2005). On the response of the oceanic wind-driven circulation to atmospheric CO_2 increase. *Climate dynamics 25*(4), 415–426.

Sætre, R. (2007). *The Norwegian coastal current: oceanography and climate*. Trondheim: Tapir Academic Press Institute of Marine Research.

Schmitz, K. S. (2018). *Physical Chemistry: Multidisciplinary Applications in Society*. Elsevier.

Schulz, H. and M. Zabel (2006). Marine geochemistry: 2 nd revised, updated and extended edition.

Strunk, A., J. Olsen, H. Sanei, A. Rudra, and N. K. Larsen (2020). Improving the reliability of bulk sediment radiocarbon dating. *Quaternary Science Reviews 242*, 106442.

Svendsen, J. I., H. Alexanderson, V. I. Astakhov, I. Demidov, J. A. Dowdeswell, S. Funder, V. Gataullin, M. Henriksen, C. Hjort, M. Houmark-Nielsen, et al. (2004). Late Quaternary ice sheet history of northern Eurasia. *Quaternary Science Reviews 23*(11-13), 1229–1271.

Svendsen, J. I. and J. Mangerud (1987). Late Weichselian and Holocene sea-level history for a cross-section of western Norway. *Journal of Quaternary Science 2*(2), 113–132.

Wang, L., W. Zhu, J. Xie, L. Li, and C. Zhang (2015). Study of the shear strength of sediments in main sedimentation stages. *Marine Georesources & Geotechnology 33*(6), 556–566.

Webb, K. E., Ø. Hammer, A. Lepland, and J. S. Gray (2009). Pockmarks in the inner Oslofjord, Norway. *Geo-Marine Letters 29*(2), 111–124.